UCLouvain

École polytechnique de Louvain

Diffusion MRI-Based Analysis of Structural Connectivity and Its Association with Cognitive Decline in Alzheimer's Disease

Author: **Valentine Lahy**
Supervisors: **Benoit Macq, Laurence Dricot**
Readers: **Nicolas Delinte, Christophe De Vleeschouwer**
Academic year 2025–2026
Master [120] in Biomedical Engineering

Acknowledgements

I would first like to sincerely thank my supervisors, Benoît Macq and Laurence Dricot, for their guidance, support, and valuable advice throughout this master's thesis. I am grateful for the opportunity they gave me to work on such an interesting and stimulating research topic.

I would especially like to thank Nicolas Delinte for his constant availability and invaluable help throughout this project. His explanations, technical expertise, and regular support were essential to the completion of this work. I am particularly grateful for the considerable amount of time he dedicated to helping me understand the different methodological and analytical aspects of the project.

I would also like to thank the clinical and research teams at Cliniques Universitaires Saint-Luc for providing access to the dataset used in this study and for sharing their expertise regarding the clinical assessments and cognitive measures collected as part of the cohort. Their explanations of the neuropsychological tests and cognitive scores were invaluable for understanding and interpreting the data used throughout this work.

I would also like to thank my family for their continuous encouragement and support throughout the entire process.

Finally, I would like to thank everyone who contributed, directly or indirectly, to this work and to the completion of my studies.

Abstract

Alzheimer's disease is increasingly recognized as a disorder affecting large-scale brain networks rather than isolated brain regions. The objective of this study was to investigate structural connectivity alterations associated with disease progression and cognitive decline using diffusion magnetic resonance imaging (dMRI) and tractography. Whole-brain structural connectomes were reconstructed from participants classified as cognitively normal (CN), mild cognitive impairment (MCI), or dementia. Global connectivity, network-specific connectivity within the default mode, salience, and central executive networks, associations between individual structural connections and cognitive performance, and graph-theoretical metrics were analyzed. Global connectivity showed only modest differences across diagnostic groups. At the network level, significant alterations were observed within the salience network, whereas no significant group effects were detected in the default mode or central executive networks. Edge-wise analyses identified several structural connections associated with cognitive performance, particularly involving parietal, occipital, temporal, and limbic regions. Furthermore, graph-theoretical analyses revealed reduced node strength, clustering coefficient, and closeness centrality, together with increased betweenness centrality in MCI and dementia participants, suggesting a progressive reorganization of brain network topology. Overall, these findings support the hypothesis that Alzheimer's disease is associated with specific alterations of structural brain networks that are more readily detected at the level of subnetworks, individual connections, and topological properties than through global connectivity measures alone.

List of Abbreviations

Aβ	Amyloid-β
AAL	Automated Anatomical Labeling
ADC	Apparent Diffusion Coefficient
AD	Alzheimer's Disease
AxD	Axial Diffusivity
CEN	Central Executive Network
CN	Cognitively Normal
CSF	Cerebrospinal Fluid
CSD	Constrained Spherical Deconvolution
dMRI	Diffusion Magnetic Resonance Imaging
DMN	Default Mode Network
DTI	Diffusion Tensor Imaging
DWI	Diffusion-Weighted Imaging
FA	Fractional Anisotropy
FDR	False Discovery Rate
FOD	Fiber Orientation Distribution
FOV	Field Of View
MCI	Mild Cognitive Impairment

MD	Mean Diffusivity
MMSE	Mini-Mental State Examination
MRI	Magnetic Resonance Imaging
MSMT-CSD	Multi-shell Multi-Tissue Constrained Spherical Deconvolution
OLS	Ordinary Least Squares
RD	Radial Diffusivity
SD	Standard Deviation
SIFT	Spherical-Deconvolution Informed Filtering of Tractograms
SN	Salience Network
SNR	Signal-to-Noise Ratio
TE	Echo Time
TR	Repetition Time

List of Figures

1.1 Illustration of amyloid-β plaques and neurofibrillary tangles 5
1.2 Temporal evolution of major biomarkers and clinical changes in AD 6
1.3 Illustration of the relation between DMN, SN and CEN 7
1.4 Main regions of the DMN 7
1.5 Microanatomy of white matter 9

2.1 Illustration of diffusion encoding using pulsed magnetic field gradients 13
2.2 Illustration of the two different types of diffusion (isotropic and anisotropic) in brain tissue 15
2.3 Ellipsoid used to represent each voxel for DTI 16
2.4 Illustration of the four DTI-derived metrics on MRI data 17
2.5 Comparison between DTI and CSD-based diffusion modeling 18
2.6 Example of whole-brain tractography 19
2.7 Comparison of tractography approaches: deterministic and probabilistic 20
2.8 Overview of the tractometry pipeline 23
2.9 Example of a structural brain network representation 24
2.10 Illustration of the construction of a structural connectivity matrix . 25
2.11 Illustration of the graph-theoretical metrics used in this study . . . 26
2.12 Schematic illustration of major affected white matter fiber bundles . 27

3.1 Overview of the analysis pipeline used in this study 31
3.2 Example of MRI data before and after preprocessing 36
3.3 Example of whole-brain probabilistic tractography from a participant included in the dataset 37
3.4 Illustration of AAL Atlas and example of connectivity matrix . . . 39

4.1 Distribution of cognitive scores across diagnostic groups and visits . 46
4.2 Effect of covariates on global mean structural connectivity 47
4.3 Global connectivity across diagnostic groups before and after covariate adjustment 48
4.4 Regions included in the DMN 49

4.5 DMN connectivity across diagnostic groups before and after covariate adjustment 50
4.6 Regions included in the SN 51
4.7 SN connectivity across diagnostic groups before and after covariate adjustment 51
4.8 Regions included in the CEN 52
4.9 CEN connectivity across diagnostic groups before and after covariate adjustment 52
4.10 Visualization of the most significant white matter tracts associated with cognitive scores 55
4.11 Examples of posterior occipito-parietal pathways 56
4.12 Examples of language-related pathways 56
4.13 Examples of fronto-striatal pathways 57
4.14 Example of a memory-related pathway 57
4.15 Comparison of graph-theoretical metrics across diagnostic groups . 59

5.1 Corpus callosum anatomy 64
5.2 Language-related anatomical tracts 65
5.3 Cingulum bundle 67

List of Tables

2.1 Main differences between SIFT and SIFT2 22

3.1 Availability of cognitive scores across participants 34
3.2 MRI acquisition parameters across participants 35
3.3 AAL regions included in each functional network 41

4.1 Number of significant tracts surviving FDR correction for each cognitive score 54
4.2 Top significant structural connections associated with cognitive scores after FDR correction 54

5.1 Tracts associated with posterior interhemispheric and visuo-parietal pathways 63
5.2 Tracts associated with language-related temporo-frontal and temporo-parietal pathways 64
5.3 Tract associated with fronto-striatal and subcortical pathways . . . 65
5.4 Tracts associated with sensorimotor and fronto-parietal pathways . 66
5.5 Tracts associated with limbic and memory-related pathways 67

A.1 Summary of missing data and participant exclusions 82

B.1 Post-hoc Tukey HSD comparisons between diagnostic groups for cognitive scores 84
B.2 Post-hoc Tukey HSD comparisons of global mean connectivity . . . 85
B.3 Post-hoc Tukey HSD comparisons of DMN connectivity 85
B.4 Post-hoc Tukey HSD comparisons of SN connectivity 85
B.5 Post-hoc Tukey HSD comparisons of CEN connectivity 86
B.6 Post-hoc Tukey HSD comparisons for mean strength 86
B.7 Post-hoc Tukey HSD comparisons for mean clustering coefficient . . 86
B.8 Post-hoc Tukey HSD comparisons for mean closeness centrality . . . 87
B.9 Post-hoc Tukey HSD comparisons for mean betweenness centrality . 87

C.1 Selected significant structural connections for the Executive score. . 88

C.2 Selected significant structural connections for the Global cognition score. 89
C.3 Selected significant structural connections for the Language score. . 89
C.4 Selected significant structural connections for the Memory score. . . 89
C.5 Selected significant structural connections for the MMSE score. . . 90
C.6 Selected significant structural connections for the Visuospatial score. 90

Contents

Acknowledgements i
Abstract ii
List of Abbreviations iii
List of Figures v
List of Tables vii

Introduction **1**

I State of the Art **3**

1 Alzheimer's Disease **4**
1.1 Pathophysiological Mechanisms 4
1.2 From Localized Cortical Degeneration to Network Disease 6
1.3 White Matter Alterations in Alzheimer's Disease 8
1.4 The Myelin Vulnerability Hypothesis 10
1.5 Structural Connectivity in Alzheimer's Disease 11

2 Theoretical Concepts **12**
2.1 Background on Diffusion MRI 12
2.1.1 Principles of Diffusion-Weighted Imaging 12
2.1.2 Isotropic and Anisotropic Diffusion 14
2.1.3 Mathematical Modeling of Diffusion 15
2.2 Tractography 18
2.2.1 Deterministic Versus Probabilistic Algorithms 19
2.2.2 Limitations of Tractography and SIFT(2) Correction 20
2.2.3 Tractometry 22
2.3 Structural Connectivity Matrices 23
2.4 Graph-Theoretical Analysis of Brain Networks 25
2.5 Previous Diffusion MRI and Connectome Studies 27

II Analysis of Alterations in White Matter Related to Cognitive Decline 30

3 Materials and Methods 31
3.1 Dataset and Participants . . . 32
3.1.1 Participants . . . 32
3.1.2 Cognitive Assessment . . . 33
3.2 MRI Data Acquisition and Preprocessing . . . 35
3.3 Whole-Brain Tractography . . . 37
3.4 Connectivity Matrices . . . 38
3.5 Statistical Analyses . . . 40

4 Results 45
4.1 Distribution of Cognitive Scores . . . 45
4.2 Global and Network-Level Connectivity . . . 47
4.2.1 Global Connectivity across diagnostic groups . . . 48
4.2.2 Network-Level Connectivity . . . 49
4.2.3 Summary of Findings . . . 53
4.3 Tract-Based Analysis . . . 53
4.4 Graph-Theoretical Metrics . . . 58

5 Discussion 61
5.1 Results Interpretation . . . 61
5.1.1 Global and Network-Level Connectivity Findings . . . 61
5.1.2 Tract-Based Analyses . . . 63
5.1.3 Graph-Theoretical Analyses . . . 68
5.2 Limitations and Methodological Considerations . . . 69

Conclusion 71

Bibliography 72

A Inventory: Missing Data 82

B Cognitive Scores: p-values Comparisons 84

C Significant Tracts 88

Introduction

Alzheimer's disease is a progressive neurodegenerative disorder and the most common cause of dementia worldwide. It is characterized by a gradual and irreversible decline in cognitive functions, initially affecting episodic memory and subsequently impairing language, executive functions, and visuospatial abilities. This clinical progression is accompanied by a progressive loss of autonomy, leading to increasing dependence in activities of daily living.[1, 2]

However, clinical manifestations correspond only to a relatively advanced stage of the pathological process. Neuropathological findings and biomarker studies indicate that cerebral alterations begin several years before clinical symptoms become apparent, typically five to seven years (and in some cases considerably longer). This preclinical phase has become a central focus of research, both for understanding the underlying pathophysiological mechanisms and for developing early diagnostic and therapeutic strategies.[1, 2]

Beyond its individual clinical impact, Alzheimer's disease represents a major global public health challenge. According to the World Health Organization, dementia is the seventh leading cause of death worldwide and one of the primary causes of disability among older adults. Recent estimates indicate that approximately 55 to 60 million people currently live with dementia globally, of whom nearly 70% are affected by Alzheimer's disease. In the absence of curative treatment, this number is projected to reach 82 million by 2030 and exceed 152 million by 2050. In Europe alone, more than 10 million individuals are affected, including over one million in France and more than 200,000 in Belgium. Prevalence increases exponentially with age, doubling approximately every five years after the age of 65. Women are disproportionately affected, largely due to their longer life expectancy.[1, 2]

Long misinterpreted as a form of accelerated aging, Alzheimer's disease is now recognized as a distinct pathological entity driven by specific pathophysiological mechanisms.[1] Historically, it has been conceptualized primarily as a gray matter disorder, characterized by extracellular accumulation of β-amyloid (Aβ) peptides,

formation of neurofibrillary tangles composed of hyperphosphorylated tau protein, and progressive cortical atrophy, particularly in the hippocampus and medial temporal cortex. This framework gave rise to the "amyloid cascade hypothesis", which dominated research for several decades by postulating amyloid deposition as the initiating event in disease progression.[3] However, the limited clinical efficacy of therapeutic strategies exclusively targeting amyloid has progressively challenged this explanatory model.[4]

Over the past two decades, accumulating evidence from neuropathological and neuroimaging studies has demonstrated early and significant alterations in cerebral white matter in Alzheimer's disease. These findings suggest that white matter involvement may not simply be a secondary consequence of cortical neuronal degeneration, but rather an active contributor to cognitive decline. Consequently, Alzheimer's disease is increasingly understood as a disorder of distributed brain networks, involving disruptions in structural and functional connectivity rather than being confined to localized cortical damage.[5]

The aim of this thesis is to critically examine current knowledge regarding structural and microstructural alterations of white matter in Alzheimer's disease, to explore the underlying pathophysiological mechanisms that may account for these changes, and to evaluate their clinical and methodological implications, particularly in the context of advanced neuroimaging approaches and network-based analyses.

This thesis is organized into two main parts. The first part provides a comprehensive review of current knowledge on white matter alterations in Alzheimer's disease, as well as the theoretical foundations of diffusion MRI, tractography, and structural connectivity analysis. The second part presents the methodological framework, results, and discussion of the present study, which investigates structural connectivity alterations associated with cognitive decline.

Tools such as ChatGPT were occasionally used for language editing and sentence reformulation. All scientific content was produced by the author.

Part I

State of the Art

Chapter 1

Alzheimer's Disease

In order to understand why the study of white matter is particularly relevant in Alzheimer's disease (AD), it is first essential to examine the underlying pathophysiological mechanisms occurring in the affected brain. This chapter presents the main biological processes involved in the disease and discusses the vulnerability of white matter, highlighting the importance of investigating structural connectivity alterations.

1.1 Pathophysiological Mechanisms

AD is characterized by two major neuropathological hallmarks: the accumulation of amyloid plaques and the formation of neurofibrillary tangles (see Figure 1.1).

Amyloid-β Plaques

Amyloid plaques are extracellular deposits primarily composed of highly insoluble amyloid-β (Aβ) peptides. These aggregates are widely considered one of the earliest pathological events in AD. Aβ peptides are produced through the proteolytic cleavage of the Amyloid Precursor Protein (APP), a transmembrane protein expressed in neurons. This cleavage occurs through the sequential action of two enzymes, β-secretase and γ-secretase enzymes, which generate Aβ fragments that are released into the extracellular space. Under pathological conditions, these Aβ peptides tend to accumulate and aggregate, forming oligomers and eventually amyloid plaques. The abnormal deposition of Aβ is thought to contribute to neuronal toxicity and to trigger a cascade of downstream pathological processes.[6, 7]

Neurofibrillary Tangles

Neurofibrillary degeneration is characterized by the accumulation of intracellular aggregates of hyperphosphorylated tau protein, known as neurofibrillary tangles. Under physiological conditions, tau is a microtubule-associated protein that stabilizes microtubules and supports axonal transport. However, in AD, tau undergoes abnormal hyperphosphorylation, which reduces its affinity for microtubules and leads to their destabilization. As a consequence, tau proteins detach from microtubules and aggregate into paired helical filaments that accumulate within neurons. This process disrupts synaptic function and impairs neuronal communication.[7, 8] Tau pathology follows a characteristic spatial progression described by the Braak staging system, initially affecting the transentorhinal cortex before spreading to limbic regions such as the hippocampus and eventually reaching widespread isocortical areas.[9]

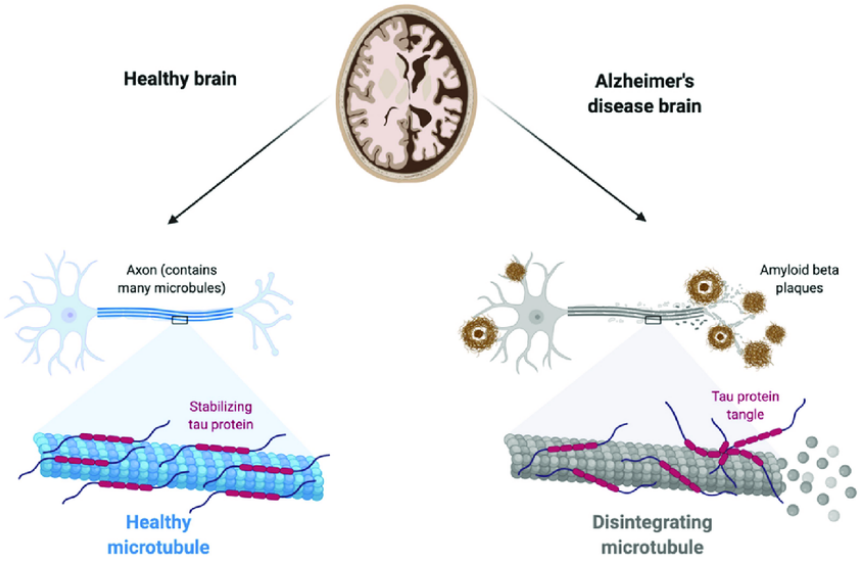


Figure 1.1: Illustration of the two main neuropathological hallmarks of AD: Aβ plaques and neurofibrillary tangles composed of tau protein.[10]

In addition to amyloid and tau pathology, AD involves several other biological processes that contribute to disease progression. Among these mechanisms, synaptic dysfunction, neuronal injury, glial activation, and vascular factors are increasingly recognized as important contributors to neurodegeneration.[11]

The progression of these pathological processes is thought to follow a characteristic temporal sequence, as illustrated in Figure 1.2. According to this hypothetical

model, amyloid-β accumulation begins very early during the preclinical stage of AD, several years before the appearance of clinical symptoms.[11]

As the disease progresses, synaptic dysfunction, tau-related neuronal injury, and structural brain alterations progressively emerge. Cognitive decline and clinical impairment appear later, once substantial biological and network alterations have already occurred. This model therefore suggests that important pathological changes may already be present long before AD becomes clinically detectable.[11]

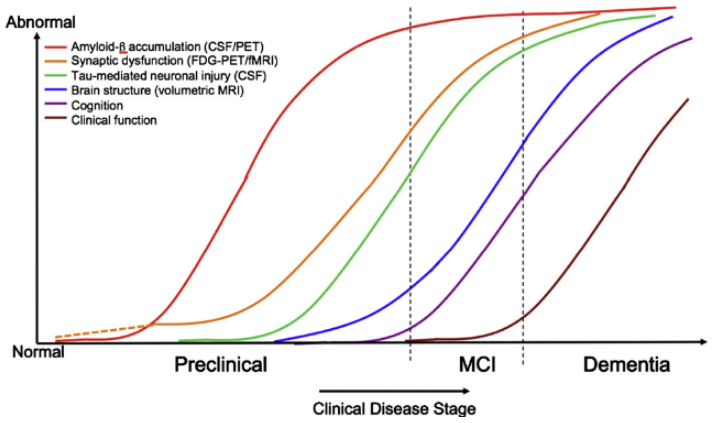


Figure 1.2: Hypothetical temporal evolution of major biomarkers and clinical changes across the progression of AD, from the preclinical stage to dementia. Amyloid-β accumulation appears early, followed by synaptic dysfunction, tau-mediated neuronal injury, structural brain changes, cognitive decline, and clinical impairment.[11]

1.2 From Localized Cortical Degeneration to Network Disease

Historically, AD was primarily described as a neurodegenerative disorder characterized by progressive gray matter atrophy, particularly in the hippocampus and medial temporal lobe, regions critically involved in memory processes. Neuroimaging studies have consistently reported structural alterations in medial temporal, paralimbic, and temporoparietal regions, which are strongly associated with the accumulation and spatial progression of tau pathology.[11, 12]

More recently, AD has increasingly been conceptualized as a disorder affecting large-scale brain networks rather than isolated cortical regions. In this network-based perspective, neurodegeneration is thought to propagate through functionally

and structurally connected brain regions. Among the large-scale brain networks involved in AD, three networks are considered particularly important: the default mode network (DMN), the salience network (SN), and the central executive network (CEN). The three networks are illustrated in Figure 1.3.

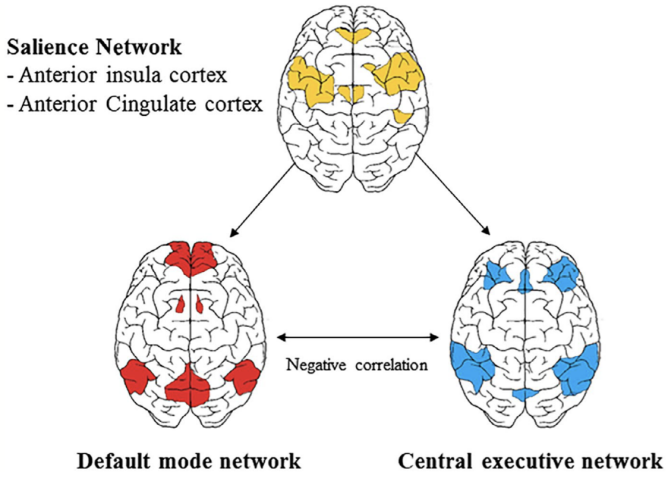


Figure 1.3: Illustration of the DMN, SN, and CEN, three major large-scale brain networks involved in cognitive functioning and frequently altered in AD.[13]

Default Mode Network

One of the networks most consistently implicated in AD is the DMN, which is illustrated in Figure 1.4. The DMN is particularly active during resting states and includes regions such as the medial prefrontal cortex, the posterior cingulate cortex, the precuneus, and the lateral temporal cortex.[12, 14]

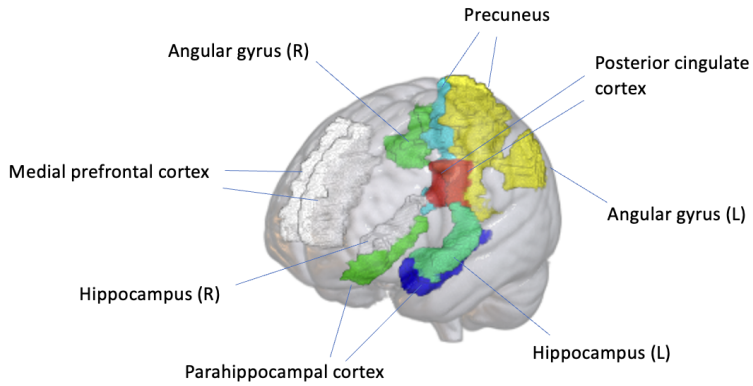


Figure 1.4: Main regions of the DMN, including the medial prefrontal cortex, posterior cingulate cortex, precuneus, angular gyri, and medial temporal structures such as the hippocampus and parahippocampal cortex.

Interestingly, the spatial distribution of Aβ deposition strongly overlaps with the regions that compose the DMN. This observation suggests that brain regions that are highly connected within functional networks may be particularly vulnerable to the spread of pathological processes. As a result, AD is increasingly viewed as a disorder affecting large-scale brain networks rather than isolated brain regions.[12]

Salience Network

The SN is mainly composed of the anterior insula and the anterior cingulate cortex. This network plays an important role in attentional control, detection of salient stimuli, and switching between different cognitive systems, particularly between the DMN and CEN, as seen in Figure 1.3.[15, 16]

Several studies have suggested that alterations of the SN may contribute to cognitive dysfunction in AD. Functional and structural abnormalities within the SN have been associated with impaired attentional processes and reduced network coordination.[15, 16]

Interestingly, some studies have reported increased functional connectivity within the SN in patients with AD and MCI. This increase in connectivity may reflect a compensatory mechanism attempting to maintain cognitive function despite the progressive disruption of other brain networks. However, it may also reflect abnormal network activity associated with disease progression.[15, 16]

Central Executive Network

The CEN includes mainly the dorsolateral prefrontal cortex and posterior parietal cortices. This network is involved in higher-order cognitive functions such as working memory, executive control, and goal-directed behavior.[17]

Disruptions of the CEN have been reported in AD and are thought to contribute to executive dysfunction and reduced cognitive flexibility.[17] Altered interactions between the CEN, DMN, and SN may further contribute to large-scale network disorganization observed during disease progression.

1.3 White Matter Alterations in Alzheimer's Disease

White matter constitutes the structural backbone of brain connectivity. It is mainly composed of oligodendrocytes and myelinated axons that enable communication between distant cortical and subcortical regions. While gray matter is primarily

involved in local information processing, white matter ensures the rapid transmission and integration of neural signals across distributed brain networks.[18, 19]

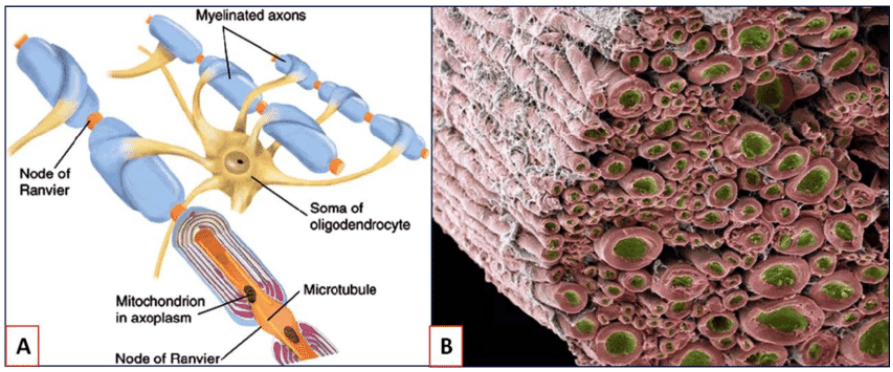


Figure 1.5: Microanatomy of white matter. (A) Schematic illustration of myelinated axons surrounded by oligodendrocytes, highlighting the myelin sheath and nodes of Ranvier. (B) Microscopic view of a cross-section of myelinated axonal fibers in white matter tissue.[20]

Figure 1.5 illustrates the anatomy of white matter. Myelinated axons are organized into structured fiber bundles, forming a highly ordered architecture. At the macroscopic level, white matter fibers are classically subdivided into three major categories [21]:

- Association fibers, which connect cortical regions within the same hemisphere and play a central role in complex cognitive functions such as memory, language, and executive processing;
- Commissural fibers, primarily represented by the corpus callosum, which enable interhemispheric communication;
- Projection fibers, which connect the cortex with deep brain structures, including the thalamus, brainstem, and spinal cord.

Growing evidence suggests that white matter is significantly affected in AD. Neuropathological studies have reported axonal degeneration, demyelination, and oligodendrocyte dysfunction in several white matter regions. These alterations may contribute to the disruption of communication between distant brain regions.[19, 22] These alterations are frequently observed in major association tracts involved in memory and cognitive functions, including the cingulum bundle, the uncinate fasciculus, the corpus callosum, and long association fibers connecting frontal, parietal, and temporal regions (see Section 2.5).

1.4 The Myelin Vulnerability Hypothesis

The myelin vulnerability hypothesis proposes that alterations of myelin and oligodendrocytes are not only secondary consequences of neuronal loss, but may play an early role in the development of neurodegenerative diseases, including AD.[19]

Contrary to earlier conceptions, myelin is not a static structure but a dynamic component that requires continuous maintenance throughout adulthood. Oligodendrocytes are responsible not only for the formation of myelin during development, but also for maintaining the myelin sheath throughout life.[23]

According to the developmental model proposed by Bartzokis (2004)[19], brain regions that are myelinated later in development, particularly the frontal and temporal lobes, may be more vulnerable to age-related degeneration. These regions contain many long-range connections and have high metabolic demands. Interestingly, they are also among the earliest regions affected in AD.[19]

At the cellular level, oligodendrocytes have limited antioxidant defenses and high energy requirements, making them particularly vulnerable to metabolic stress. Damage to these cells may compromise myelin integrity, disrupt axonal conduction, and lead to alterations in brain connectivity.[24]

Several factors contribute to this vulnerability:

- the high metabolic dependence of oligodendrocytes;[24]
- the sustained energetic demands of long-distance fibers;[19]
- the terminal vascularization of deep white matter, increasing sensitivity to chronic hypoperfusion;[25]
- the particular susceptibility of late-myelinating regions to age-related alterations.[19]

In the context of AD, these elements support the notion that myelin degradation may occur early in the pathological cascade and actively contribute to progressive network disintegration. This perspective reinforces the growing interest in white matter integrity as a potential biomarker of disease progression.[19] White matter integrity thus emerges as a central determinant of cognitive preservation, consistent with the concept of a “disconnection syndrome” described in AD.[22]

These findings highlight the importance of advanced neuroimaging techniques capable of investigating white matter microstructure in vivo. Diffusion magnetic

resonance imaging (dMRI) has therefore become a key tool for studying structural connectivity alterations associated with AD.[18, 19, 22]

1.5 Structural Connectivity in Alzheimer's Disease

The progressive reconceptualization of AD as a network-level disorder highlights the importance of examining white matter integrity beyond localized cortical atrophy. Cognitive functions such as memory and executive processing rely on distributed neural circuits rather than isolated brain regions. Consequently, disruption of structural connectivity may play a central role in cognitive decline and clinical symptoms in AD.[22]

White matter alterations, including axonal degeneration and myelin damage, may occur early during disease progression. These microstructural changes can impair communication between interconnected brain regions and progressively disrupt the integrity of large-scale neural networks. Studying white matter organization may therefore provide important insights into the mechanisms underlying cognitive decline in AD. In addition, white matter alterations have been proposed as potential imaging biomarkers for the early detection and monitoring of disease progression.[26, 27]

Diffusion MRI provides a non-invasive method for investigating white matter organization in vivo. By measuring the diffusion of water molecules within brain tissue, diffusion MRI allows indirect assessment of white matter microstructure and structural connectivity. When combined with tractography and connectome analyses, these techniques make it possible to study whole-brain structural networks and their alterations in AD.[28]

These considerations highlight the importance of advanced diffusion MRI techniques and connectome-based approaches to investigate structural connectivity alterations in AD. A more detailed overview of previous diffusion MRI, tractography and connectome studies in AD is provided in Section 2.5.

Chapter 2

Theoretical Concepts

This chapter introduces the main theoretical concepts and methodological tools required for the analysis of structural brain connectivity. It first presents the basic principles of diffusion magnetic resonance imaging, which enable the investigation of white matter microstructure in vivo. The chapter then describes the main modeling approaches used to characterize diffusion, as well as tractography techniques that allow the reconstruction of white matter pathways. Finally, the concepts of tractometry and structural connectivity matrices are introduced, providing the methodological basis for the analyses presented in the following chapters.

2.1 Background on Diffusion MRI

Diffusion Magnetic Resonance Imaging (dMRI) is a non-invasive imaging technique widely used to analyze the microstructural organization of white matter in the brain. It relies on the measurement of the random thermal motion of water molecules, known as diffusion, within biological tissues.[29–31]

2.1.1 Principles of Diffusion-Weighted Imaging

Diffusion-Weighted Imaging (DWI) can be considered as an extension of conventional MRI in which additional diffusion-encoding gradients are incorporated, in different directions, into a T2-weighted sequence. These gradients are applied after the excitation pulse and just before signal readout in order to make the MRI signal sensitive to the motion of water molecules.[30]

The first diffusion gradient introduces a spatial variation of the magnetic field, causing spins located at different positions to precess at different rates. As a result, the spins progressively dephase, as seen in Figure 2.1. A second gradient pulse, identical in strength, duration, and direction, is then applied. In theory, if the water molecules had remained stationary between the two gradients, the second pulse would perfectly reverse the effect of the first and fully rephase the spins.[30]

However, under physiological conditions, water molecules undergo random thermal motion. Because they move between the two gradient pulses, the rephasing is incomplete. This results in a loss of signal intensity, and the magnitude of this signal attenuation reflects the degree of water diffusion within the tissue.[30]

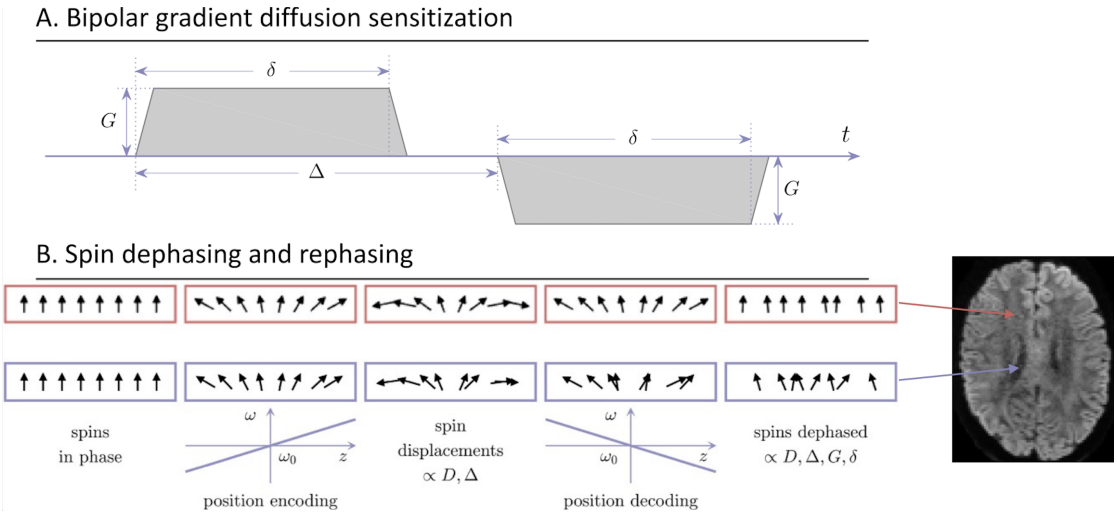


Figure 2.1: Illustration of diffusion encoding using pulsed magnetic field gradients. (A) Bipolar diffusion-sensitizing gradient scheme, showing two gradient pulses of duration δ separated by a time interval Δ. (B) Principle of spin dephasing and rephasing: if water molecules remain stationary between the two gradients, the second gradient reverses the phase dispersion induced by the first and the spins rephase. However, when diffusion occurs, molecular displacement leads to incomplete rephasing and signal attenuation.[32]

b-value

The b-value reflects the degree of diffusion weighting applied during image acquisition. A low b-value corresponds to low diffusion sensitivity and therefore minimal signal attenuation, whereas a high b-value increases diffusion weighting and leads to stronger signal attenuation.[30] The b-value is expressed in [s/mm^2] and is proportional to the square of the amplitude and the duration of the applied diffusion gradient.[29] The b-value is calculated using the following equation, known

as the Stejskal-Tanner equation:

$$b = \gamma^2 G^2 \delta^2 \left(\Delta - \frac{\delta}{3} \right),$$

where γ is the gyromagnetic ratio, G is the gradient strength, δ is the gradient duration, and Δ is the time between the gradient pulses.[29, 32]

The signal attenuation follows an exponential decay:

$$S = S_0 e^{-bD},$$

where S is the measured signal, S_0 is the signal without diffusion weighting, and D is the apparent diffusion coefficient (ADC).[30, 33]

Increasing the b-value increases the signal attenuation, which enhances diffusion contrast between white and gray matter but also reduces the signal-to-noise ratio (SNR), representing a fundamental trade-off in diffusion MRI acquisition.[30]

Apparent Diffusion Coefficient (ADC)

In biological tissues, water diffusion is hindered by cellular membranes, myelin sheaths, and other microstructural barriers. As a result, the measured diffusion coefficient does not correspond to the true self-diffusion coefficient of water, but rather to an ADC, which reflects both molecular motion and tissue microstructure.[30] The ADC is estimated from the signal attenuation observed between a non-diffusion-weighted image ($b = 0$) and a diffusion-weighted image. Variations in ADC values therefore provide indirect information about the microstructural properties of the tissue.[30]

2.1.2 Isotropic and Anisotropic Diffusion

Depending on the surrounding microstructural environment in the brain, water diffusion can be classified as isotropic or anisotropic.[29, 31] The two types of diffusion are illustrated in Figure 2.2.

Isotropic diffusion occurs when water molecules are free to move equally in all directions, as observed in cerebrospinal fluid (CSF). This type of diffusion is typically represented by a spherical diffusion profile. In contrast, anisotropic diffusion arises when molecular motion is directionally constrained. In this case, diffusion is preferential along specific orientations and is commonly represented by an ellipsoidal profile.[29]

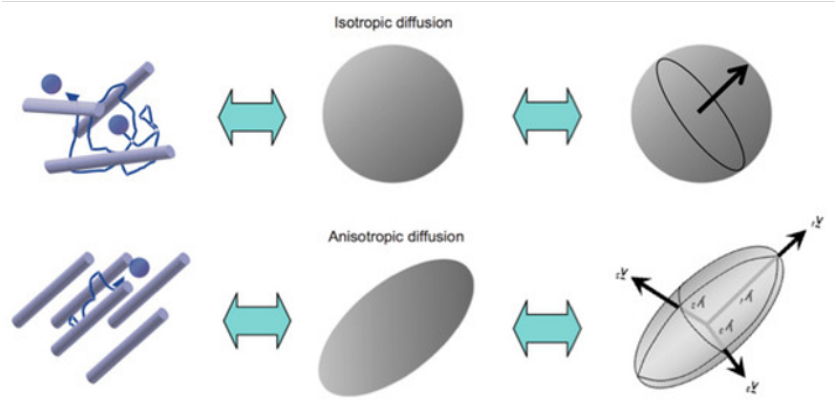


Figure 2.2: Illustration of the two different types of diffusion (isotropic and anisotropic) in brain tissue.[29]

Diffusion in white matter

In white matter, water diffusion is strongly influenced by the presence of axonal membranes and myelin sheaths, which restrict molecular displacement perpendicular to the main fiber direction. As a result, diffusion becomes anisotropic and reflects the underlying organization of axonal bundles. Consequently, diffusion MRI provides indirect but valuable information about fiber orientation and microstructural organization of the white matter. These diffusion properties are influenced by several microstructural features, including axonal density, fiber coherence, and the degree of myelinisation. [31, 33]

To extract quantitative information from diffusion-weighted images acquired along multiple directions, mathematical models are required to describe the diffusion process within each voxel.[29]

2.1.3 Mathematical Modeling of Diffusion

Mathematical models are applied to dMRI data in order to extract quantitative metrics that reflect the microstructural properties of brain tissue. Among the various diffusion models proposed in the literature, Diffusion Tensor Imaging (DTI) and Multi-Shell Multi-Tissue Constrained Spherical Deconvolution (MSMT-CSD) are widely used in the study of AD.

Diffusion Tensor Imaging (DTI)

DTI models the diffusion process within each voxel using a second-order tensor, which can be geometrically represented as an ellipsoid characterized by three eigenvalues and three corresponding eigenvectors (see Figure 2.3). The eigenvectors describe the principal diffusion directions, while the eigenvalues quantify the magnitude of diffusion along these directions.[32]

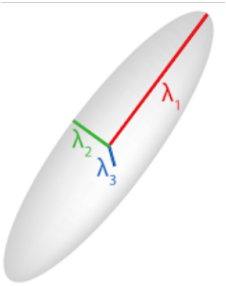


Figure 2.3: Ellipsoid used to represent each voxel for DTI.[34]

DTI allows the computation of several scalar metrics that are commonly used to characterize white matter integrity:[29, 32]

(a) **Fractional Anisotropy (FA):** quantifies the degree of diffusion anisotropy within a voxel. Higher FA values indicate more directionally constrained diffusion, which is generally associated with coherent and organized white matter fiber bundles.

$$\mathrm{FA} = \sqrt{\frac{1}{2}} \frac{\sqrt{(\lambda_1 - \lambda_2)^2 + (\lambda_1 - \lambda_3)^2 + (\lambda_2 - \lambda_3)^2}}{\sqrt{\lambda_1^2 + \lambda_2^2 + \lambda_3^2}} \tag{2.1}$$

(b) **Mean Diffusivity (MD):** represents the average diffusion magnitude across all directions. Increased MD values are often associated with tissue damage or loss of structural integrity.

$$\mathrm{MD} = \frac{\lambda_1 + \lambda_2 + \lambda_3}{3} \tag{2.2}$$

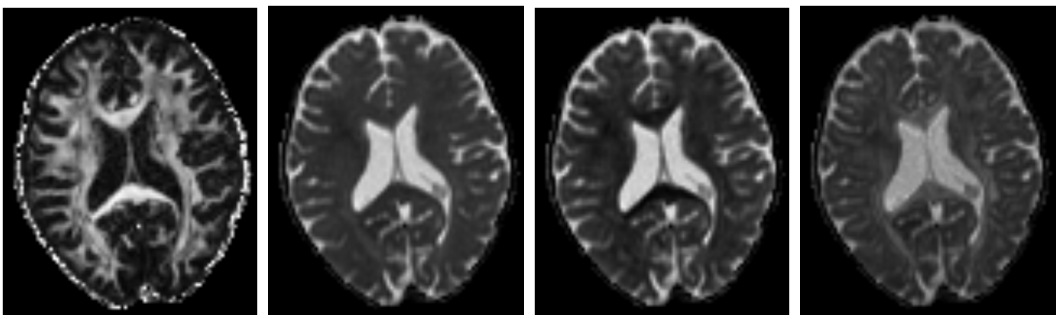
(c) **Radial Diffusivity (RD):** measures diffusion perpendicular to the principal fiber direction and has been associated with changes in myelin integrity.

$$\mathrm{RD} = \frac{\lambda_2 + \lambda_3}{2} \tag{2.3}$$

(d) **Axial Diffusivity (AxD):** reflects diffusion parallel to the principal fiber direction and has been linked to axonal integrity.

$$\mathrm{AD} = \lambda_1 \tag{2.4}$$

The four DTI-derived metrics are illustrated in Figure 2.4.



(a) **(b)** **(c)** **(d)**

Figure 2.4: Illustration of DTI-derived metrics on MRI data: (a) Fractional Anisotropy (FA), (b) Mean Diffusivity (MD), (c) Radial Diffusivity (RD), and (d) Axial Diffusivity (AxD). Images generated from the dataset used in this study.

However, a major limitation of DTI is its assumption of a single dominant fiber orientation per voxel. This simplification leads to inaccurate modeling in regions containing complex fiber configurations, such as crossing, kissing, or branching fibers, which are common in the human brain.[29, 32]

Multi-Shell Multi-Tissue Constrained Spherical Deconvolution (MSMT-CSD)

To overcome the limitations of single-tensor models, more advanced approaches have been developed to better capture complex fiber configurations within each voxel. Constrained Spherical Deconvolution (CSD) estimates the Fiber Orientation Distribution (FOD), which represents the distribution of fiber orientations within each voxel rather than a single dominant direction.[35]

Multi-Shell Multi-Tissue CSD (MSMT-CSD) extends the classical CSD framework by incorporating diffusion data acquired at multiple b-values and by modeling different tissue compartments, typically white matter, gray matter, and cerebrospinal fluid (CSF). This approach improves the separation of tissue-specific diffusion

signals and provides more accurate estimation of white matter fiber orientations, particularly in regions affected by partial volume effects.[35]

By estimating multiple fiber orientations within a single voxel, MSMT-CSD enables a more realistic representation of white matter architecture, especially in regions containing crossing fibers. As a result, MSMT-CSD has become a widely used method for dMRI tractography and connectome reconstruction in both healthy and pathological populations.[35] A comparison between DTI and CSD-based modeling in regions containing crossing fibers is illustrated in Figure 2.5.

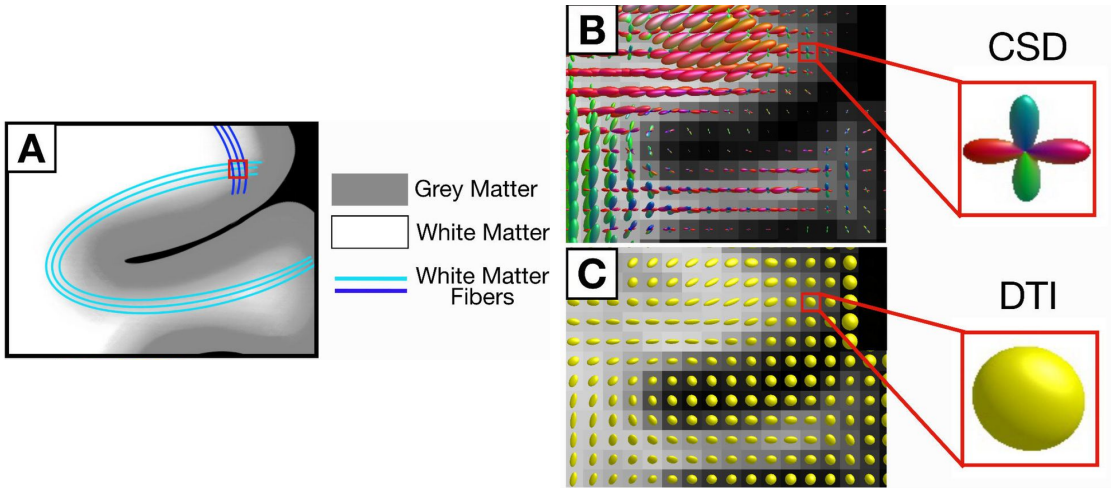


Figure 2.5: Comparison between DTI and CSD-based diffusion modeling in regions containing crossing fibers. (A) Schematic illustration of crossing white matter fibers within brain tissue. (B) CSD-based modeling allows multiple fiber orientations to be estimated within the same voxel through the FOD. (C) DTI represents diffusion using a single tensor and therefore captures only one dominant orientation within the voxel.[36]

2.2 Tractography

Based on the FODs estimated using MSMT-CSD, tractography algorithms can be applied to reconstruct white matter pathways. Tractography provides a three-dimensional representation of the trajectories of streamlines connecting different brain regions (see Figure 2.6). These streamlines do not correspond to individual axons but rather represent the most probable pathways of underlying fiber bundles inferred from the diffusion signal.[32]

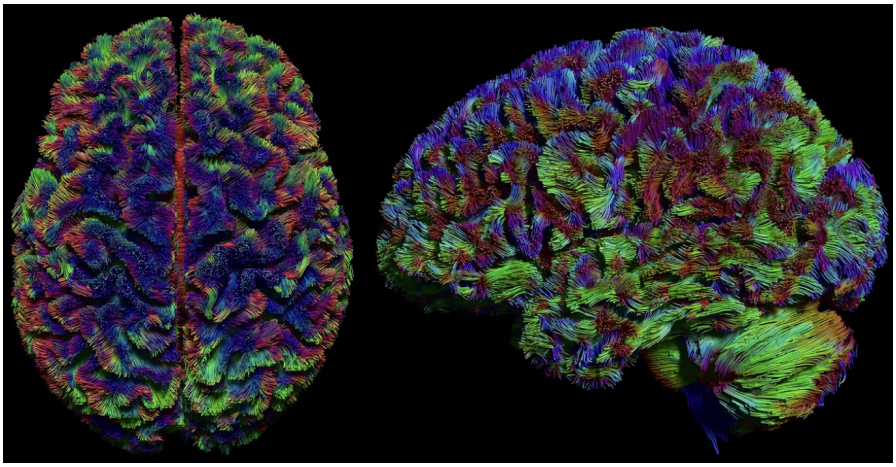


Figure 2.6: Example of whole-brain tractography (red = left-right, green = front-back, blue = top-down)[32]

2.2.1 Deterministic Versus Probabilistic Algorithms

Two main classes of tractography algorithms can be distinguished:

Deterministic tractography

Deterministic tractography propagates streamlines by following the single most prominent fiber orientation at each voxel. Starting from a seed point, the algorithm iteratively follows the principal diffusion direction until a stopping criterion is reached, such as low anisotropy, entering no-white matter, or exceeding a curvature threshold.[37, 38]

This approach typically produces smooth, thin, and anatomically well-defined tracts, as seen on Figure 2.7. Deterministic tractography is computationally efficient and relatively easy to interpret visually. However, because only one dominant orientation is followed, the method may fail in regions containing crossing, branching, or kissing fibers. As a result, deterministic approaches are more prone to false negatives and may underestimate the complexity of white matter architecture.[37, 39]

Probabilistic tractography

Probabilistic tractography addresses some of these limitations by incorporating uncertainty in fiber orientation estimation. Instead of following a single direction, streamlines are generated by repeatedly sampling from the distribution of possible fiber orientations, often derived from the FOD.[37, 38]

This approach allows a better reconstruction of pathways in regions with complex fiber configurations and improves sensitivity to less prominent fiber populations. Probabilistic tractography therefore provides a more comprehensive representation of structural connectivity. However, because many possible trajectories are generated, probabilistic approaches may also produce anatomically implausible streamlines and increase the number of false positive connections. In addition, probabilistic tractography generally requires longer computation times and produces results that can be more difficult to interpret visually compared to deterministic tractography.[38, 39]

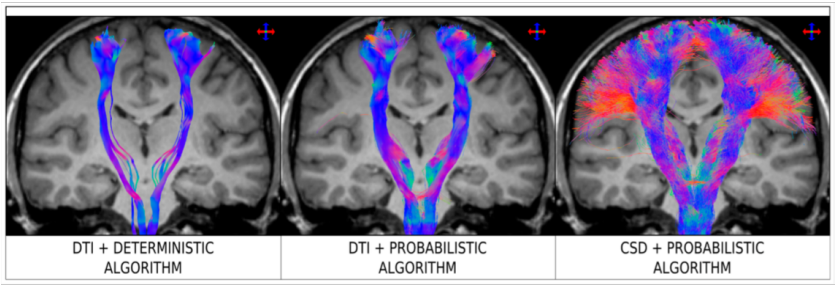


Figure 2.7: Comparison of tractography approaches. From left to right: deterministic tractography based on DTI, probabilistic tractography based on DTI, and probabilistic tractography using CSD.[38]

Overall, deterministic tractography generally provides higher anatomical specificity, whereas probabilistic tractography offers greater sensitivity in complex white matter regions. Modern connectome studies increasingly rely on probabilistic approaches combined with advanced diffusion models such as CSD in order to better capture the complexity of brain connectivity.

2.2.2 Limitations of Tractography and SIFT(2) Correction

Despite its widespread use, tractography has several inherent limitations. In particular, probabilistic tractography does not provide a direct quantitative measure of anatomical connectivity, and the resulting streamline counts can be biased.[39] This is especially problematic for fiber pathways that pass through regions of fiber crossing, dispersion, or low fractional anisotropy, such as association and commissural tracts. These tracts may be under-reconstructed or missed entirely. Conversely, pathways that are more compatible with the local diffusion model and tracking parameters may be preferentially reconstructed and therefore over-represented relative to the underlying anatomy.[40]

Additional biases may also arise from noise, partial volume effects, uncertainty in fiber orientation estimation, and the choice of tracking parameters. As a result, tractography reconstructions should be interpreted as indirect estimations of structural connectivity rather than exact anatomical representations.[40]

In studies of neurodegenerative diseases, probabilistic tractography is often preferred because of its increased sensitivity to microstructural alterations and its ability to better handle uncertainty in regions containing complex fiber configurations. However, probabilistic approaches also tend to generate a large number of streamlines, which may artificially inflate connectivity estimates and increase the number of false positive connections.[38]

To reduce these biases, post-processing approaches such as Spherical-deconvolution Informed Filtering of Tractograms (SIFT) and its weighted extension SIFT2 have been developed.[38]

SIFT

SIFT was developed to improve the biological accuracy of tractography reconstructions.[41] The method uses information derived from the FOD estimated by CSD to compare the reconstructed streamline density with the underlying diffusion signal. SIFT iteratively removes streamlines that are considered inconsistent with the diffusion model until the streamline density better matches the estimated fiber densities. As a result, the number of streamlines connecting two brain regions becomes more proportional to the underlying white matter fiber cross-sectional area, providing a more biologically meaningful estimate of structural connectivity.[41]

SIFT2

SIFT2 was later introduced as an extension of the original SIFT framework. Instead of removing streamlines, SIFT2 assigns a weighting coefficient to each streamline so that the weighted streamline densities better correspond to the diffusion signal and fiber densities estimated from the FOD. This approach preserves the entire tractogram while still improving the quantitative interpretation of connectivity measures. In neurodegenerative diseases such as AD, where structural connectivity alterations may be subtle and spatially distributed, preserving less prominent pathways may be particularly important.[42]

The main differences between SIFT and SIFT2 are summarized in Table 2.1.

Feature	SIFT	SIFT2
Principle	Removes streamlines to match streamline density with the diffusion model	Assigns weights to streamlines without removing them
Streamline preservation	Requires discarding a large proportion of generated streamlines	Preserves the entire tractogram
Computational cost	Computationally demanding due to the need for very large tractograms	More computationally efficient
Connectivity estimation	Reduces tractography biases but may lose information from weaker pathways	Provides weighted quantitative connectivity estimates while preserving subtle pathways
Reproducibility	More sensitive to random tractography variability	Generally provides more stable and reproducible connectivity measures
Suitability for connectomics	Less suited for dense whole-brain connectome analyses	Particularly suited for quantitative connectome analysis

Table 2.1: Main differences between SIFT and SIFT2.[41, 42]

2.2.3 Tractometry

Tractometry is an analysis approach that focuses on specific white matter bundles and allows the quantification of dMRI measures along anatomically defined pathways. Unlike voxel-wise analyses or global connectivity approaches, tractometry aims to characterize microstructural properties along an entire fiber bundle reconstructed through tractography, while preserving the spatial information along its trajectory.[32]

Conceptually, tractometry involves several main steps, as seen in Figure 2.8. First, a bundle of interest is extracted from a whole-brain tractogram using anatomically guided segmentation methods. Then, a representative centerline (often called a "core streamline") is defined in order to standardize the sampling along the tract. Diffusion-derived metrics, such as FA, MD, RD, AD, or other microstructural indices, are then projected and sampled along this trajectory. This process results in a longitudinal profile of the bundle, commonly referred to as a "bundle profile". Finally, these profiles can be statistically compared between subjects or groups.[32]

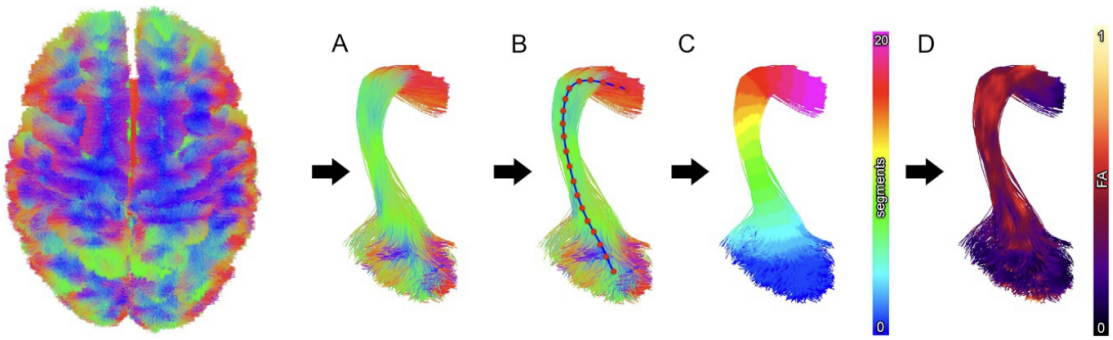


Figure 2.8: Overview of the tractometry pipeline. (A) Extraction of a white matter bundle from whole-brain tractography. (B) Definition of a representative core streamline. (C) Segmentation of the bundle along its trajectory. (D) Sampling of diffusion-derived measures along the tract to generate a bundle profile.[32]

This approach has several methodological advantages. It provides better anatomical specificity than voxel-based analyses, since the analysis is restricted to streamlines belonging to a specific bundle. It also makes it possible to detect localized alterations that could be hidden when averaging values across an entire tract or when using connectivity measures reduced to a single value per connection. In neurodegenerative diseases such as AD, where microstructural damage may be heterogeneous and unevenly distributed along a tract, this spatial sensitivity is particularly valuable.

However, tractometry strongly depends on the quality of tractography reconstruction and accurate bundle segmentation. Errors in bundle definition or in alignment between subjects may introduce artificial variability in the resulting profiles. In addition, point-by-point analysis along a tract raises the issue of multiple comparisons, which requires appropriate statistical correction methods.[32]

Overall, tractometry can be considered as a complementary approach to global connectome analyses, providing a more detailed and spatially resolved investigation of white matter microstructural integrity.

2.3 Structural Connectivity Matrices

The brain can be modeled as a complex network in which brain regions are represented as nodes and white matter connections as edges (see Figure 2.9). Prior to constructing connectivity matrices, the brain is typically divided into a set of regions using an anatomical parcellation defined by a brain atlas. Each region of the atlas cor-

responds to a node of the network, while the white matter connections reconstructed by tractography define the edges between nodes.[**skoch2016connectivity**]

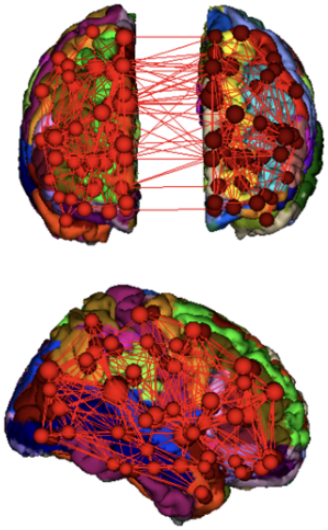


Figure 2.9: Example of a structural brain network representation. Brain regions defined by an anatomical atlas are represented as nodes, while the connections between regions derived from tractography are represented as edges.[**skoch2016connectivity**]

Using the connections reconstructed by tractography, this network representation enables the construction of structural connectivity matrices, which provide a compact and quantitative description of inter-regional structural connectivity.

Figure 2.10 illustrates how a structural connectivity matrix is constructed. The rows and columns of the matrix correspond to the different brain regions defined by a given anatomical atlas. Each element of the matrix represents the strength of the connection between a pair of regions.[**skoch2016connectivity**] Structural connectivity matrices are typically symmetric, since the connection between region A and region B is equivalent to the connection between region B and region A. The size of the matrix depends on the number of regions defined in the atlas. For an atlas containing N regions, the resulting connectivity matrix has dimensions N $\times$ N.

Structural connectivity matrices can be weighted using different metrics, such as streamline count, mean fractional anisotropy along reconstructed pathways, or streamline weights derived from filtering procedures such as SIFT. Higher values in the matrix generally indicate stronger structural connectivity between two brain regions, although the specific interpretation depends on the weighting measure

used.

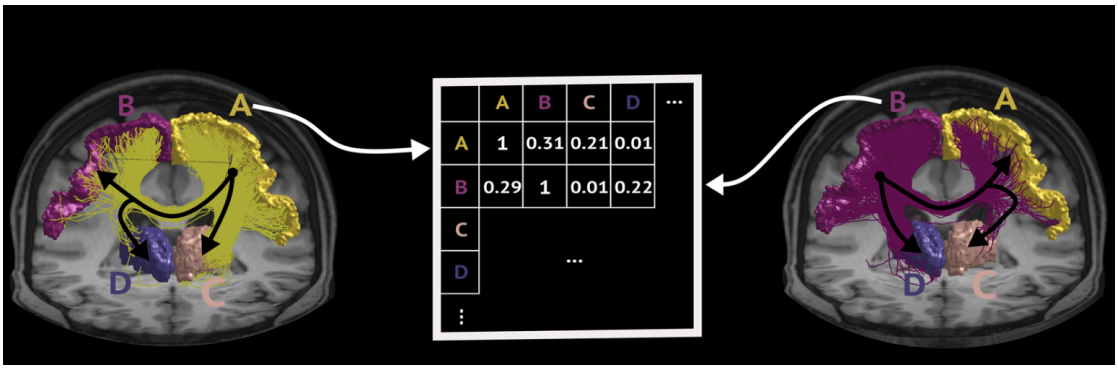


Figure 2.10: Illustration of the construction of a structural connectivity matrix. Brain regions defined by an anatomical atlas are considered as nodes, and the white matter connections between them are represented as edges. These connections can be summarized in a connectivity matrix, where each element represents the strength of connectivity between two regions.[**skoch2016connectivity**]

2.4 Graph-Theoretical Analysis of Brain Networks

Structural connectivity matrices can be further analyzed using graph theory, a mathematical framework commonly used to study the organization of complex networks. Within this framework, the network representation introduced previously can be represented as a graph in which brain regions correspond to nodes and structural connections correspond to edges (see Figure 2.9).[43, 44]

Graph-theoretical analyses provide quantitative measures describing different aspects of brain network organization, including connectivity strength, local segregation, global integration, and the relative importance of specific brain regions within the network. These methods are widely used in dMRI studies of AD because they allow the investigation of large-scale alterations in structural connectivity beyond isolated white matter tracts.[43, 44]

In the present study, several nodal graph-theoretical metrics were investigated, including node strength, clustering coefficient, closeness centrality, and betweenness centrality. Figure 2.11 presents a schematic illustration of these metrics.

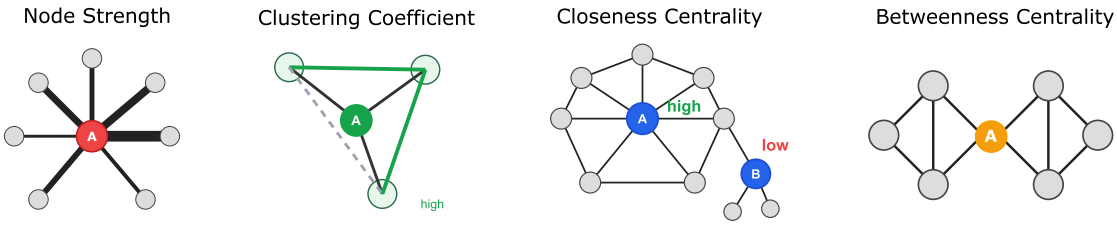


Figure 2.11: Illustration of the graph-theoretical metrics used in this study: node strength, clustering coefficient, closeness centrality, and betweenness centrality.

Node Strength

Node strength corresponds to the sum of the connection weights linked to a given node.[45] In brain connectomes, a high node strength indicates that a region is strongly and directly connected to many other brain regions. Regions with high node strength are generally considered highly connected hubs that may play an important role in large-scale communication and information integration across the brain.[28]

Clustering Coefficient

The clustering coefficient reflects the degree to which neighboring nodes are interconnected, thereby forming local clusters.[46] For an individual node, it corresponds to the fraction of existing connections between its neighboring nodes relative to the maximum number of possible connections between them.[45] High clustering coefficient values indicate stronger local network organization and segregation. In the brain, this property is thought to support specialized local information processing within functionally related regions.

Closeness Centrality

Closeness centrality measures how efficiently a node communicates with the rest of the network through short paths. It is defined as the inverse of the average shortest path length between a given node and all other nodes of the network.[28, 45] Nodes with high closeness centrality can rapidly exchange information with distant brain regions through short communication paths. This metric is therefore often used to identify regions that play an important role in large-scale network integration.[28]

Betweenness Centrality

Betweenness centrality quantifies how frequently a node lies on the shortest paths connecting other pairs of nodes in the network.[45] It therefore reflects the role of a node as a bridge or relay between different parts of the network. Nodes

with high betweenness centrality are often considered important connector hubs involved in global information transfer and network integration.[28, 46] Because of their strategic position within the network, alterations affecting these regions may strongly disrupt communication efficiency and overall brain network organization.

2.5 Previous Diffusion MRI and Connectome Studies in Alzheimer's Disease

Diffusion MRI alterations in Alzheimer's disease

Over the past two decades, dMRI has been widely used to investigate white matter alterations associated with AD. Numerous studies have reported widespread microstructural abnormalities reflected by changes in diffusion-derived metrics. In particular, patients with AD typically show decreased FA and increased MD, suggesting reduced white matter integrity potentially related to axonal degeneration and demyelination. Increased RD has also frequently been reported and is often interpreted as a marker of myelin disruption.[27, 47]

Microstructural alterations are not uniformly distributed across the brain but preferentially affect regions involved in memory and higher cognitive functions. Damage is particularly pronounced in structures such as the hippocampus, entorhinal cortex, and cingulum. Early signs of structural disconnection have also been reported in the splenium of the corpus callosum and the fornix. In addition, major association pathways such as the superior longitudinal fasciculus and the uncinate fasciculus, which connect frontal and temporal regions, have been shown to be affected.[27] These white matter pathways are illustrated in Figure 2.12.

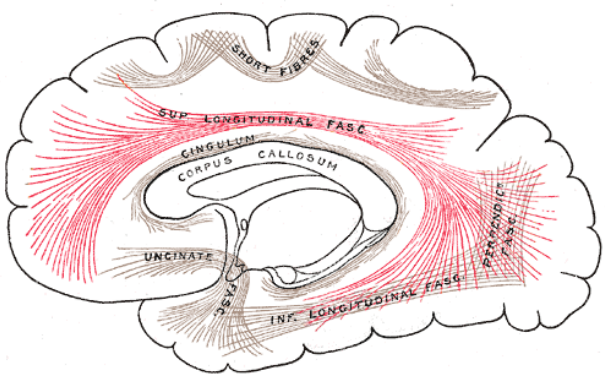


Figure 2.12: Illustration of major affected white matter fiber bundles, including the corpus callosum, cingulum, uncinate fasciculus, and longitudinal association fibers.[48]

Importantly, several studies have shown that these microstructural alterations are associated with cognitive decline. Damage to the fornix, cingulum, and uncinate fasciculus has been linked to impairments in episodic memory, whereas alterations in long association tracts have been associated with deficits in executive functioning, attention, and processing speed.[27, 47]

Tractography and connectome-based studies

Beyond voxel-wise diffusion analyses, tractography has increasingly been used to reconstruct white matter pathways and investigate large-scale structural connectivity in AD. Using tractography-derived connectivity matrices, several studies have demonstrated disrupted structural communication between cortical and subcortical regions in cognitively impaired individuals.[49, 50]

These approaches are particularly relevant in AD because cognitive impairment is increasingly thought to result from progressive disruption of communication between distributed brain regions rather than isolated focal lesions.

Connectome-based approaches have shown that AD is associated with altered organization of large-scale brain networks rather than isolated white matter damage. Structural connectivity studies have reported reduced connectivity within posterior associative regions, including the precuneus, posterior cingulate cortex, parietal regions, and temporal association cortices. These regions are considered important hubs of structural and functional brain communication and are frequently implicated in AD.[12, 49]

Several connectome and functional connectivity studies have further shown that AD preferentially affects large-scale cognitive networks such as the DMN, the CEN, and the SN. In particular, reduced connectivity within the DMN has been consistently reported, especially in posterior regions including the precuneus and posterior cingulate cortex, which are considered major hubs of brain communication.[12, 44] Alterations of the CEN have also been associated with executive dysfunction and impaired cognitive control, while abnormal SN activity has been proposed to reflect compensatory or maladaptive network reorganization during disease progression.[15]

Graph-theoretical studies in Alzheimer's disease

Several studies have investigated graph-theoretical properties of structural brain networks in AD. Using graph-theoretical analyses, previous studies have reported reduced global efficiency, decreased clustering coefficient, disrupted small-world organization, and altered hub connectivity in patients with AD.[44, 51, 52]

These findings suggest that neurodegeneration affects not only individual white matter tracts but also the global topology and communication efficiency of large-scale structural brain networks. Interestingly, some studies have suggested that network alterations may already be detectable during the mild cognitive impairment (MCI) stage, supporting the hypothesis that structural disconnection occurs progressively throughout disease evolution.[44, 51]

Methodological limitations and motivation for the present study

Despite these advances, several methodological limitations remain. Many diffusion MRI studies still rely on simplified diffusion models such as DTI, which may inadequately represent complex fiber configurations in regions containing crossing fibers. In addition, tractography and connectome-based analyses remain sensitive to methodological choices such as atlas selection, tractography algorithms, thresholding strategies, and network construction methods.[53]

These limitations highlight the importance of advanced tractography and connectome-based approaches for improving the characterization of structural connectivity alterations associated with cognitive decline and AD. In particular, advanced diffusion models and quantitative connectome analyses may provide a more accurate representation of large-scale white matter organization in neurodegenerative diseases.

Part II

Analysis of Alterations in White Matter Related to Cognitive Decline

Chapter 3

Materials and Methods

This chapter describes the data and methodology used in this study to investigate structural connectivity alterations associated with Alzheimer's disease.

An overview of the complete analysis pipeline is illustrated in Figure 3.1.

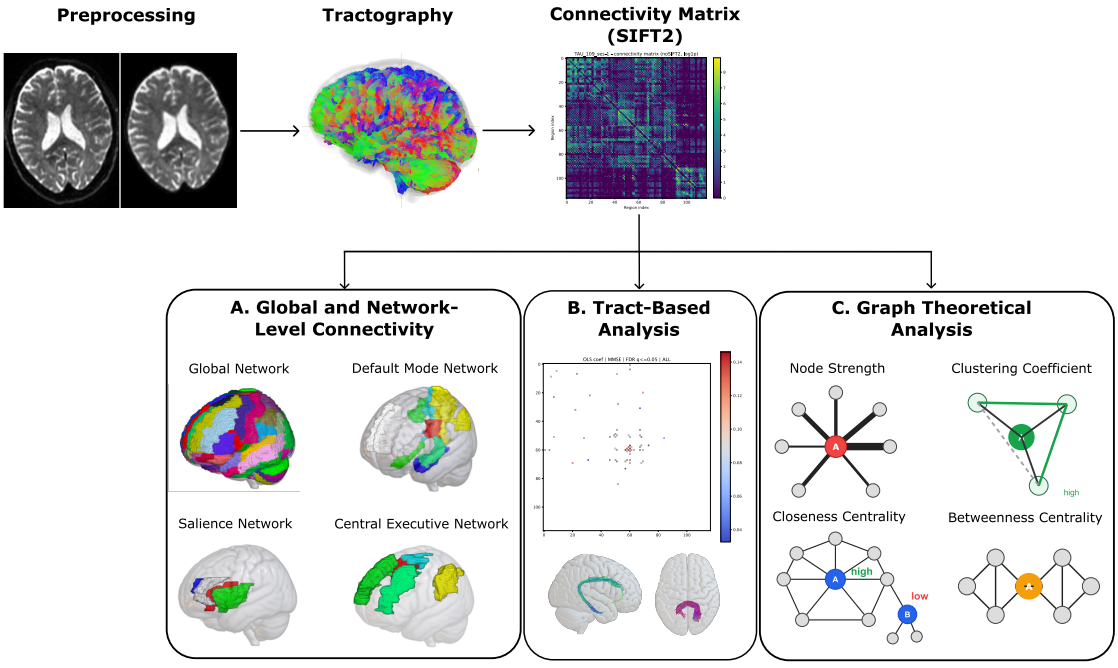


Figure 3.1: Overview of the analysis pipeline used in this study. Diffusion MRI data were processed to generate whole-brain tractography and structural connectivity matrices, which were used in subsequent analyses, including **A.** global and network connectivity, **B.** tract-based analysis, and **C.** graph-theoretical metrics.

The analysis pipeline begins with dMRI preprocessing, followed by whole-brain probabilistic tractography based on FODs. Structural connectivity matrices are then constructed using SIFT2-weighted streamline counts.

The resulting connectivity data were then analyzed through three complementary approaches. First, global and network-level measures were computed to assess large-scale connectivity alterations. Second, a tract-based analysis was performed to identify specific connections associated with cognitive scores. Finally, graph-theoretical metrics were used to analyze the topological organization of the brain network at the nodal level.

The following sections describe in detail the dataset, cognitive assessments, MRI preprocessing steps, and statistical analyses performed in this study.

3.1 Dataset and Participants

3.1.1 Participants

This study initially included 186 participants across different stages of cognitive decline. The original dataset comprised multiple diagnostic categories, which were grouped for this study into three main categories: cognitively normal (CN), mild cognitive impairment (MCI), and dementia.

Thirteen participants were excluded due to missing MRI data or incomplete clinical information. The final cohort therefore consisted of 173 participants. The number of subjects included in each analysis may vary slightly depending on data availability for specific variables such as cognitive scores (see Table 3.1 and Appendix A for more details).

The demographic characteristics of the cohort were as follows:

- **Diagnostic group:** 65 CN, 78 MCI, and 28 patients with dementia (including Alzheimer's and non-Alzheimer's etiologies);
- **Sex:** 89 women and 82 men;
- **Education level:** from 6 to 25 years (mean ± SD: 15.7 ± 3.8 years; available for 164 participants).
- **Age:** ranged from 46.8 to 98.1 years (mean ± SD: 70.8 ± 8.8 years); Age at the time of MRI acquisition was computed as the difference between the

MRI scan date and the date of birth.

- **Amyloid status:** CN: 9 Aβ-, 6 Aβ+ and 50 unknown; MCI: 31 Aβ-, 34 Aβ+ and 15 unknown; Dementia: 8 Aβ-, 18 Aβ+ and 2 unknown.

Each participant could have one or multiple MRI visits. In this study, analyses were performed at the visit level, treating each visit as an independent observation. This study was conducted using a cross-sectional design, where each observation corresponds to a subject at a given MRI visit, and analyses were performed across subjects rather than modeling longitudinal changes within individuals.

Age, sex, and education variables were included as covariates in subsequent statistical analyses to control for potential confounding effects.

3.1.2 Cognitive Assessment

For each participant, neuropsychological assessments were conducted to evaluate their performance in multiple cognitive domains commonly affected in AD, including memory, executive functions, language, and visuospatial abilities.

Several cognitive scores were available, including the Mini-Mental State Examination (MMSE) as well as domain-specific composite scores. For each cognitive domain, participants performed three related neuropsychological tasks. The composite score corresponded to the average performance across these tasks and was subsequently expressed as a standardized Z-score relative to a reference population.

Mini-Mental State Examination (MMSE): The MMSE is a widely used global cognitive test composed of 30 questions evaluating several cognitive functions, including orientation, memory, attention, calculation, language, and visuoconstructive abilities. The total score ranges from 0 to 30, with lower scores indicating greater cognitive impairment.

Memory composite: The memory composite score was mainly based on episodic memory assessments, including the Free and Cued Selective Reminding Test (FCSRT). Participants were required to encode and recall words immediately and after a delay. The composite score incorporated immediate recall, free recall, and delayed recall performances.

Executive composite: Executive functioning was evaluated using tests assessing cognitive flexibility, processing speed, and reasoning abilities. In particular, trail-making tasks requiring sequential or alternating connections between numbers and letters were used. Additional pattern completion tasks were also included.

Language composite: Language abilities were assessed using verbal fluency and naming tasks. Category fluency and letter fluency tests required participants to generate words belonging to a semantic category or beginning with a specific letter within a limited time. Oral naming abilities were additionally evaluated using picture naming tasks.

Visuospatial composite: Visuospatial abilities were evaluated using clock-drawing and figure-copying tasks. Participants were required to complete or reproduce geometric figures and clock representations, assessing visuospatial organization and visuoconstructive abilities.

Global cognitive composite: A global cognitive composite score was calculated by averaging the available Z-scores across all cognitive domains, providing an overall measure of cognitive performance.

Z-scores were computed relative to a reference population, allowing normalization of cognitive performance across individuals. Lower Z-scores indicate poorer cognitive performance, whereas higher values reflect better cognitive functioning. The number of participants varies across cognitive domains because some scores were missing for certain participants. The global cognitive composite could still be computed when partial cognitive data were available. A summary of the number of subjects available for each cognitive measure is provided in Table 3.1.

Cognitive score	**Number of participants (N)**
MMSE	154
Memory composite	148
Executive composite	146
Language composite	150
Visuospatial composite	150
Global cognitive composite	148

Table 3.1: Availability of cognitive scores across participants.

These cognitive measures were used to quantify cognitive impairment and to investigate the relationship between white matter structural connectivity and cognitive decline.

All data were collected at Cliniques Universitaires Saint-Luc in Belgium.

3.2 MRI Data Acquisition and Preprocessing

All MRI scans were acquired on a 3T GE SIGNA^{TM} Premier scanner (GE Healthcare, Chicago, IL). T1-weighted images were acquired using closely related 3D anatomical protocols across participants, with minor variations in acquisition parameters. Diffusion MRI data were acquired using the same multi-shell diffusion protocol (`Opt_DTI_4B_64_32 HB3`) across participants. A total of 167 volumes were acquired, including 160 diffusion-weighted volumes distributed across four b-values and 7 interspersed b0 images. All acquisition parameters are summarized in Table 3.2.

Parameter	**T1-weighted MRI**	**Diffusion MRI**
Scanner	3T GE SIGNA Premier	3T GE SIGNA Premier
TE	2.36–2.97 ms	77.4–80.7 ms
TR	2118–2189 ms	4532–4842 ms
TI	400–900 ms	–
Flip angle	8–11°	90°
Voxel size (after preprocessing)	1 mm isotropic	$2 \times 2 \times 2$ mm^3
FOV	256×256 mm^2	220×220 mm^2
Matrix size	–	110×110
Number of slices	156	68
Total volumes	–	167
DW volumes	–	160
b0 images	–	7
b-values	–	1000, 2000, 3000, 5000 s/mm^2
Directions	–	64 (b1000), 32 (b2000), 32 (b3000), 32 (b5000)
Gradient duration (δ)	–	22.9 ms
Gradient separation (Δ)	–	35.7 ms
Max gradient strength	–	68.9 mT/m
Multiband factor	–	3

Table 3.2: MRI acquisition parameters across participants.

Preprocessing

Preprocessing of dMRI data was performed using the Elikopy pipeline.[54, 55] Several preprocessing steps were applied in order to improve image quality and reduce acquisition-related artifacts prior to diffusion modeling and tractography:

- **Brain extraction:** non-brain tissues were removed using Otsu thresholding. This method automatically determines an intensity threshold to separate brain tissue from surrounding structures.[54, 56]
- **Thermal denoising:** dMRI data were denoised using the random matrix theory-based method proposed by Veraart et al.[57] This approach reduces random noise while preserving the underlying anatomical diffusion signal.
- **Eddy-current and motion correction:** corrections for eddy-current distortions and subject motion were performed using the `eddy` tool from FSL (v6.0.7.8).[58, 59] This step improves the spatial alignment of diffusion-weighted volumes and reduces geometric distortions.
- **Susceptibility distortion correction:** susceptibility-induced distortions were corrected using Synb0-DISCO.[60] This method synthesizes a distortion-free b0 image from the T1-weighted anatomical image and improves the alignment between diffusion and anatomical data.

These preprocessing steps were applied to ensure high-quality diffusion data and improve the reliability of downstream analyses. An example of MRI data before and after preprocessing is shown in Figure 3.2.

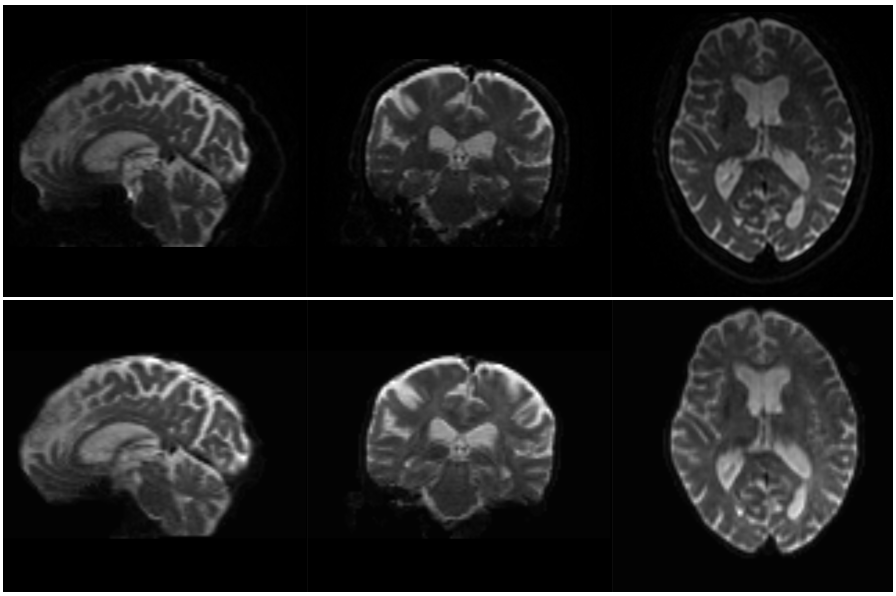


Figure 3.2: Example of MRI data before (top) and after (bottom) preprocessing with sagittal (left), coronal (middle) and axial (right) view.

3.3 Whole-Brain Tractography

Whole-brain tractography was performed using the Elikopy framework based on white matter fiber orientation distributions estimated with MSMT-CSD.[35, 61] The local diffusion model used for tractography was therefore based on multi-tissue fiber orientation distributions, allowing the reconstruction of complex fiber configurations.

Tissue response functions were estimated as part of the Elikopy MSMT-CSD processing pipeline prior to FOD estimation.[61] Whole-brain probabilistic tractography was then performed using the iFOD2 algorithm implemented in MRtrix3 [62], with the brain mask used as the tracking mask. For each subject, 1,000,000 streamlines were generated using a maximum angle of 15° and an FOD amplitude cutoff of 0.1.

Prior to tractography, the availability of the required input data, including diffusion images, white matter FODs, and brain masks, was verified. Subjects with missing files or failed processing were automatically excluded from downstream analyses. The number of excluded subjects and the corresponding reasons for exclusion are reported in Appendix A.

The resulting tractograms were saved in both `.trk` and `.tck` formats and were subsequently used for structural connectivity matrix construction and tract-based analyses. An example of whole-brain tractography is shown in Figure 3.3.

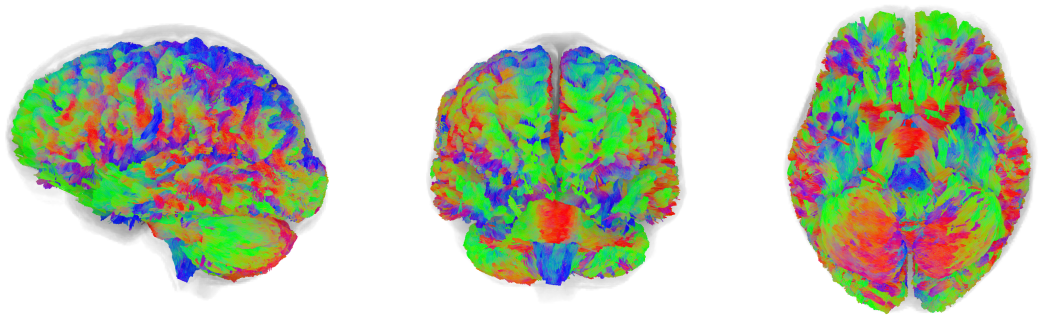


Figure 3.3: Example of whole-brain probabilistic tractography from a participant included in the dataset. Sagittal (left), coronal (middle), and axial (right) views are shown. Colors indicate the principal orientation of white matter pathways: red = left–right, green = anterior–posterior, and blue = superior–inferior.

3.4 Connectivity Matrices

Structural connectivity was represented as a network in which brain regions correspond to nodes and white matter connections to edges. For this study, the brain was parcellated into 116 cortical and subcortical regions using the Automated Anatomical Labeling (AAL) atlas defined in MNI space (see Figure 3.4a). The AAL atlas was selected because it is a widely used anatomical parcellation scheme in structural connectivity and graph-theoretical studies, facilitating the interpretation and comparison of results across studies.

Connectivity matrices were computed using custom Python scripts ([63]) based on the `NumPy`, `NiBabel`, `DIPY` [64], `Matplotlib`, `regis` [65], and `unravel` [66] libraries. The required inputs for each subject included the FA image, the whole-brain tractogram, the brain mask, and the AAL atlas.

To ensure anatomical correspondence between atlas regions and diffusion data, the AAL atlas was transformed from MNI/template space to each subject's diffusion space. First, a registration was estimated between the FA template associated with the atlas and the subject-specific FA image using the `regis` library. For the SIFT2-weighted connectivity matrices, an affine registration was used with a multi-resolution optimization scheme of 1000, 100, and 10 iterations. The resulting transformation was then applied to the AAL label image using nearest-neighbor label interpolation, in order to preserve integer anatomical labels.

This transformation allowed to associate each voxel in the subject-specific diffusion space with an AAL region. The resulting subject-specific label volume was then used to assign anatomical labels to streamline endpoints during connectivity matrix construction.

Whole-brain tractography was used to reconstruct white matter pathways. For each streamline, the anatomical labels of its two endpoints were identified, and connections between regions were defined based on these endpoint pairs. This endpoint-based approach assumes that streamlines connecting two regions reflect underlying structural connectivity between these regions.

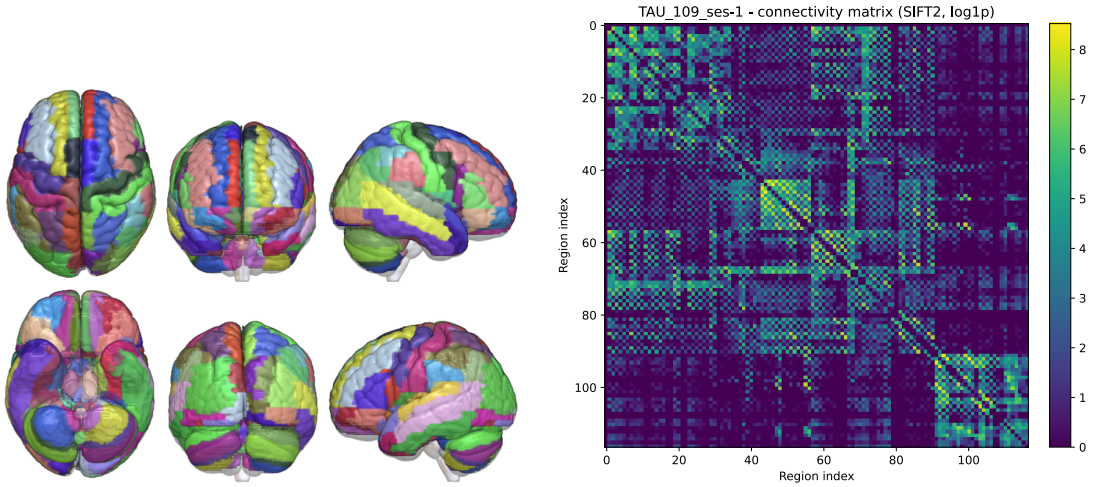
For each subject, a structural connectivity matrix was constructed using all labels from the AAL atlas, resulting in matrices of size 117×117. To ensure consistency across subjects, matrices were forced to include all atlas labels, with absent connections filled with zeros. The background label (label 0) was excluded from analysis by setting the corresponding row and column to zero.

Two types of connectivity matrices were computed:

- **Unweighted matrices:** connectivity strength was defined as the number of streamlines connecting each pair of regions.
- **SIFT2-weighted matrices:** connectivity strength was defined as the sum of streamline weights obtained using MRtrix3 `tcksift2`. Each streamline contribution was weighted by its SIFT2 coefficient and scaled by the proportionality factor μ, resulting in a biologically more meaningful estimate of connection strength.

In both cases, connectivity matrices were symmetric, reflecting the undirected nature of structural connections between brain regions.

These matrices provide a quantitative and subject-specific representation of structural brain connectivity and were used as the basis for all subsequent statistical analyses. An example of a SIFT2-weighted matrix is shown in Figure 3.4b.



(a) **(b)**

Figure 3.4: (a) AAL Atlas of 116 regions used as reference for connectivity matrices.[67] (b) Example of a subject-specific structural connectivity matrix (log-transformed for visualization). Each element represents the SIFT2-weighted connectivity strength between two brain regions defined by the AAL atlas.

3.5 Statistical Analyses

To investigate the relationship between structural connectivity and cognitive performance, analyses were conducted at multiple complementary levels.

First, connectivity was assessed at both the global (whole-brain) level and the network level, focusing on major functional networks including the default mode network (DMN), the salience network (SN), and the central executive network (CEN). Second, a tract-based analysis was performed to identify specific region-to-region connections associated with cognitive scores. Finally, graph-theoretical metrics were computed to characterize network organization at the nodal level.

All analyses were performed while controlling for potential confounding effects of age, sex, and education level.

A. Global and Network-Level Connectivity

Global and network-level connectivity were analyzed to compare structural connectivity across diagnostic groups (CN, MCI, and dementia). All analyses were performed using SIFT2-weighted connectivity matrices. To reduce skewness and stabilize variance, connectivity values were log-transformed using a $\log(1+x)$ transformation. For each subject, global mean connectivity was defined as the average of all positive upper-triangular elements of the connectivity matrix, excluding the diagonal and the background label.

In addition to whole-brain connectivity, network-specific connectivity was computed for three large-scale functional networks: the default mode network (DMN), the salience network (SN), and the central executive network (CEN). For each network, mean connectivity was computed as the average of the positive upper-triangular elements within the submatrix corresponding to the AAL regions assigned to that network. The AAL regions included in each network are listed in Table 3.3.

DMN	SN	CEN
Frontal_Sup_Medial_L	Insula_L	Frontal_Mid_L
Frontal_Sup_Medial_R	Insula_R	Frontal_Mid_R
Cingulum_Post_L	Cingulum_Ant_L	Parietal_Inf_L
Cingulum_Post_R	Cingulum_Ant_R	Parietal_Inf_R
Hippocampus_L		SupraMarginal_L
Hippocampus_R		SupraMarginal_R
ParaHippocampal_L		
ParaHippocampal_R		
Angular_L		
Angular_R		
Precuneus_L		
Precuneus_R		

Table 3.3: AAL regions included in each functional network.

Diagnostic groups were defined using the clinical classification available in the dataset and were grouped into CN, MCI, and dementia. Amyloid status was additionally extracted for visualization purposes using cerebrospinal fluid (CSF) amyloid-β 1–42 concentrations obtained through lumbar puncture. Participants with amyloid-β 1–42 values below 437 pg/mL were considered amyloid-positive.

Unadjusted group comparisons were first performed to compare global and network-level connectivity across diagnostic groups. Welch's t-tests were used for pairwise comparisons between groups. In addition, ordinary least squares (OLS) regression models were fitted to assess group effects.

To control for potential confounding effects, adjusted OLS regression models were fitted using age, sex, and education level as covariates:

$$\text{Connectivity} \sim \text{Group} + \text{Age} + \text{Sex} + \text{Education}. \tag{3.1}$$

The effects of covariates (age, sex, and education) were then removed from the connectivity values using a linear model. The residuals were then added to the mean connectivity value to obtain adjusted measures, allowing clearer visualization of group differences while accounting for potential confounding effects.

B. Tract-Based Analysis

An edge-wise analysis was performed to identify specific structural connections

associated with cognitive performance. SIFT2-weighted connectivity matrices were used for this analysis. Before statistical modelling, connectivity values were log-transformed using a $\log(1 + x)$ transformation.

For each cognitive score, including MMSE, memory, executive, visuospatial, language, and global cognitive composite scores, each edge of the connectivity matrix was tested independently. For each pair of regions i and j, an OLS regression model was fitted:

$$\text{Connectivity}_{ij} \sim \text{Score} + \text{Age} + \text{Sex} + \text{Education}. \tag{3.2}$$

Here, Connectivity_{ij} represents the log-transformed SIFT2-weighted connectivity between regions i and j. Age, sex, and education level were included as covariates. The regression coefficient associated with the cognitive score was used to quantify the direction and strength of the association between connectivity and cognitive performance.

Only edges with at least 20 available subjects and non-zero variance across subjects were included in the analysis. The analysis was performed for the whole cohort and, when sample size allowed, separately within the CN, MCI, and dementia groups.

To correct for multiple comparisons across all tested edges, p-values obtained from the edge-wise models were adjusted using the Benjamini–Hochberg False Discovery Rate (FDR) procedure. The resulting FDR-adjusted p-values are reported as q-values, and edges were considered statistically significant when $q \leq 0.05$.

$$p_{(i)} \leq \frac{i}{m}\, q \tag{3.3}$$

where $p_{(i)}$ denotes the i-th smallest p-value, m the total number of tests, and q the desired false discovery rate. This procedure controls the expected proportion of false positives among the significant results.

Selection of Significant Connections and Tract Extraction

Significant connections were selected from the edge-wise analysis using three criteria: FDR-corrected statistical significance ($q \leq 0.05$), positive regression coefficient, and sufficient SIFT2-weighted connectivity in a representative subject. Only connections with a positive regression coefficient were retained, corresponding to associations where lower cognitive performance was associated with reduced structural connectivity. This choice was motivated by the focus on connectivity loss associated with cognitive decline.

Specifically, edges were retained if their connectivity value was greater than 10 in the subject-specific SIFT2-weighted matrix.

For each cognitive score, candidate connections were ranked by increasing q-value, and up to 15 top-ranking edges were selected for tract extraction. For visualization, tract extraction was performed in a representative subject (`TAU_109_ses-1`) using DIPY. For each selected edge, the two corresponding AAL regions were used as region-of-interest masks. Streamlines were first filtered to include those passing through the first region and then further filtered to retain only streamlines also passing through the second region. The resulting streamlines were saved as individual tract files for visualization and downstream tract-specific analyses.

C. Graph-Theoretical Analysis

Finally, graph-theoretical analyses were performed to characterize the organization of structural brain networks. For each subject, the SIFT2-weighted connectivity matrix was interpreted as a weighted, undirected graph, where AAL regions corresponded to nodes and structural connections corresponded to weighted edges.

Before graph construction, the diagonal and the background label were set to zero. Connectivity values were log-transformed using a $\log(1+x)$ transformation in order to reduce the influence of extremely high connectivity weights and improve the distribution of connectivity values across the network. No additional thresholding was applied, except for removal of the background node.

Four graph-theoretical metrics were computed using the `NetworkX` Python library [68]:

- **Node strength**: the sum of weighted connections of a node, reflecting its overall structural connectivity.
- **Clustering coefficient**: reflects the tendency of neighboring nodes to form interconnected clusters and therefore provides an estimate of local connectivity density.
- **Closeness centrality**: quantifies how close a node is to all other nodes in the network and is often interpreted as an indicator of communication efficiency.
- **Betweenness centrality**: quantifies how frequently a node lies on the shortest paths between other nodes, reflecting its potential role in information transfer across the network.

For shortest-path based metrics, connection weights were converted to distances using the inverse of the connectivity strength, so that stronger structural connections corresponded to shorter graph distances.

Graph metrics were first computed at the nodal level for each AAL region. Subject-level summary measures were then obtained by averaging each metric across all brain regions, excluding the background label.

Diagnostic group differences in subject-level graph metrics were assessed by comparing CN, MCI, and dementia groups. Unadjusted OLS models were first fitted using diagnostic group as the only predictor. Adjusted OLS models were then fitted including age, sex, and education level as covariates:

$$\text{Graph metric} \sim \text{Group} + \text{Age} + \text{Sex} + \text{Education}. \tag{3.4}$$

Adjusted graph metric values were also computed by removing the effects of age, sex, and education using residuals from covariate-only models and adding back the mean value of the original metric.

Graph metrics were computed using custom Python scripts ([63]) based on `NumPy`, `Pandas`, `NetworkX`, and `Statsmodels`.

Chapter 4

Results

This section presents the results of the analyses investigating differences in structural connectivity between diagnostic groups and their relationship with cognitive performance. Results are organized according to the different levels of analysis described in the Methods section. First, global and network-level connectivity measures are reported, followed by edge-wise analyses identifying specific connections associated with cognitive scores. Finally, graph-theoretical metrics are presented to characterize alterations in network organization at the nodal level.

All results are presented both before and after adjustment for age, sex, and education, when applicable. For group-comparison figures, the p-value displayed on each plot corresponds to the global effect of diagnostic group. This global p-value indicates whether an overall difference exists among CN, MCI, and dementia participants, but does not specify which pairs of groups differ significantly. Post-hoc Tukey HSD comparisons were therefore performed, and the corresponding adjusted p-values for pairwise group comparisons are reported in Appendix B.

4.1 Distribution of Cognitive Scores

To verify whether cognitive performance decreased with disease progression, cognitive scores were compared across diagnostic groups. Cognitive performance was assessed in the CN, MCI, and dementia groups using the MMSE and composite scores for memory, language, visuospatial, executive, and global cognitive performance.

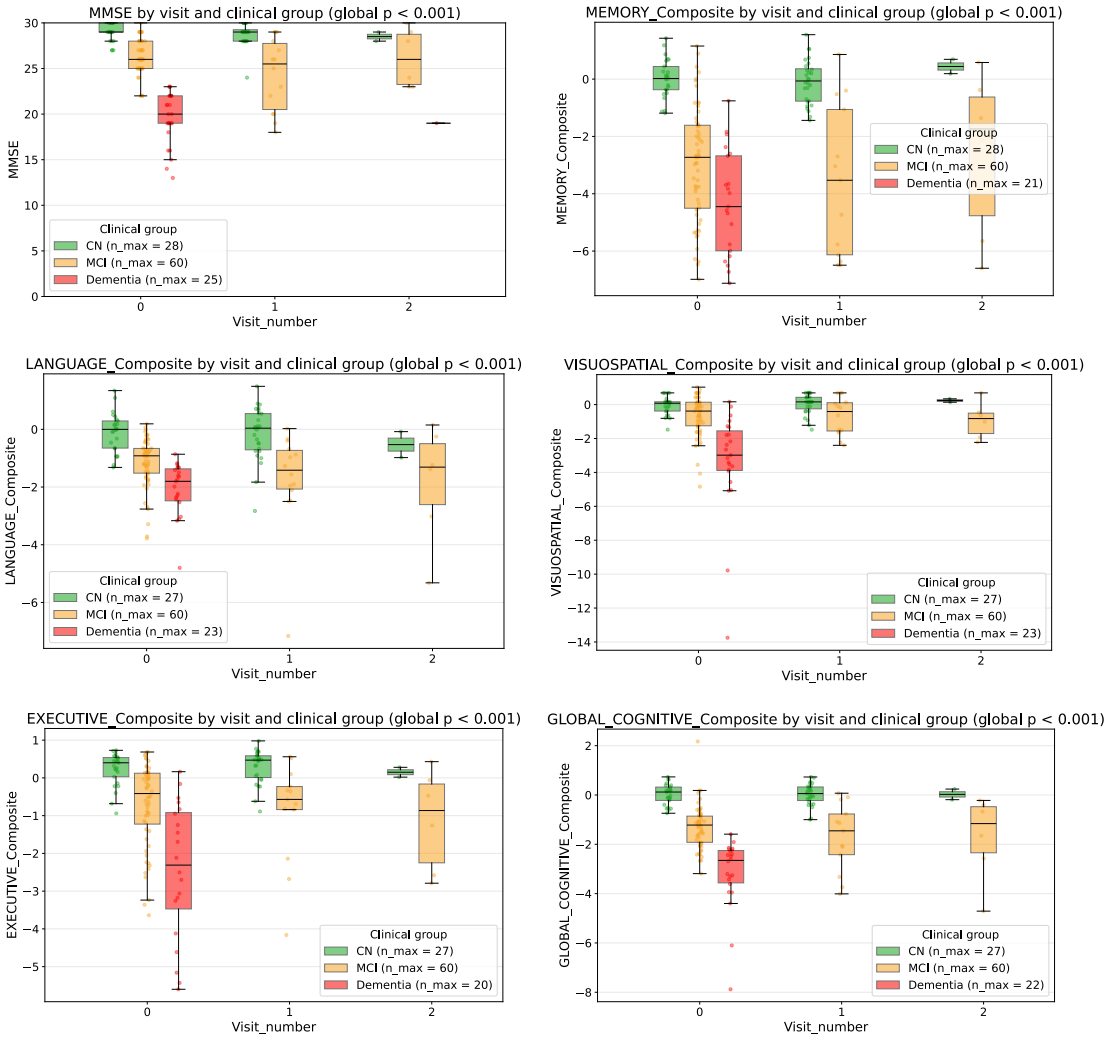


Figure 4.1: Distribution of cognitive scores across diagnostic groups and visits. The six panels show MMSE (top-left), Memory composite (top-right), Language composite (middle-left), Visuospatial composite (middle-right), Executive composite (bottom-left), and Global cognitive composite scores (bottom-right). Green: CN participants, orange: MCI participants, and red: participants with dementia. Boxplots represent score distributions across visits, with individual data points overlaid.

As shown in Figure 4.1, clear and statistically significant differences ($p < 0.001$) in cognitive scores were observed across diagnostic groups. CN participants consistently performed the highest scores across all domains, whereas dementia participants showed the lowest performance. MCI participants displayed intermediate values between CN and dementia groups.

Post-hoc Tukey HSD analyses revealed significant pairwise differences between diagnostic groups for all cognitive scores (Appendix B.1). For visuospatial performance, the difference between CN and MCI participants was weaker ($p = 0.021$) but remained statistically significant.

Variability in cognitive performance appeared greater in the MCI group compared with CN participants, reflecting the heterogeneity of this intermediate clinical stage. Dementia participants also showed increased variability in some cognitive domains.

4.2 Global and Network-Level Connectivity

Effect of covariates on global connectivity

The influence of age, sex, and education on global structural connectivity was evaluated prior to group comparisons and is illustrated in Figure 4.2.

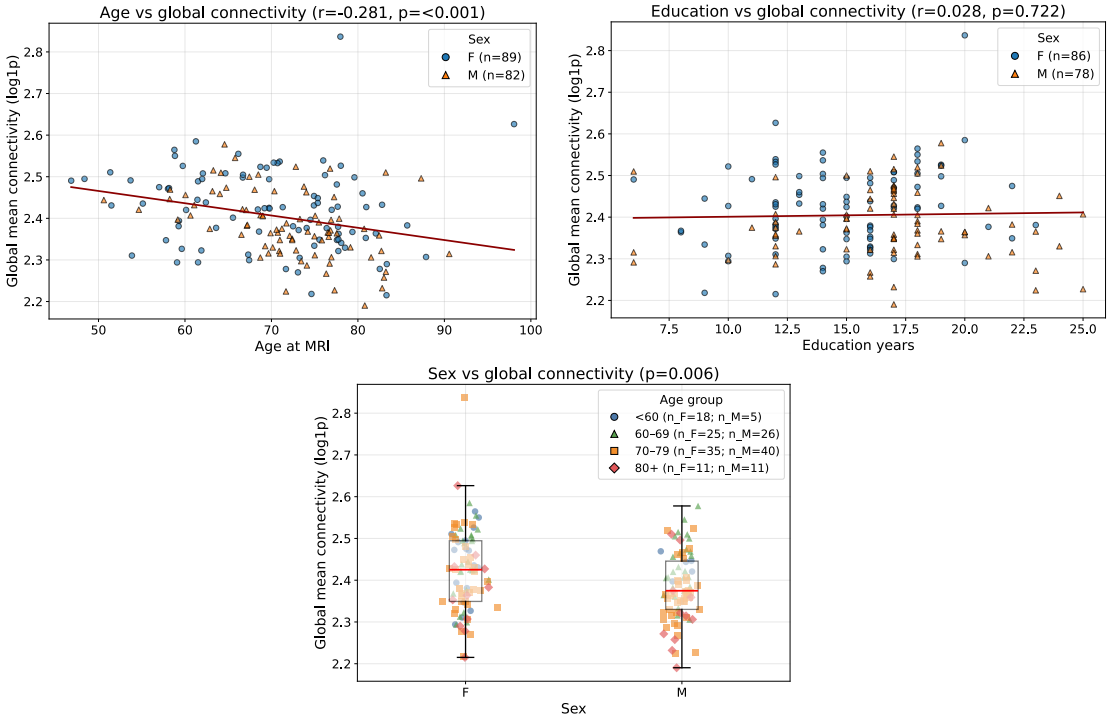


Figure 4.2: Effect of covariates on global mean structural connectivity. Top-left: age versus connectivity (points colored by sex). Top-right: education years versus connectivity (points colored by sex). Bottom: connectivity by sex (points colored by age group). Regression lines are shown where applicable.

A significant negative correlation was observed between age and global connectivity ($r = -0.281$, $p < 0.001$), indicating that older participants tended to exhibit lower mean structural connectivity values. In addition, a significant effect of sex on global connectivity was observed ($p = 0.006$), with differences in connectivity distributions between male and female participants.

By contrast, no significant association was found between education level and global connectivity ($r = 0.028$, $p = 0.722$). Nevertheless, education was still included as a covariate in subsequent analyses to maintain consistency in the statistical model.

4.2.1 Global Connectivity across diagnostic groups

Figure 4.3 presents whole-brain structural connectivity across the CN, MCI, and dementia groups before and after adjustment for age, sex, and education.

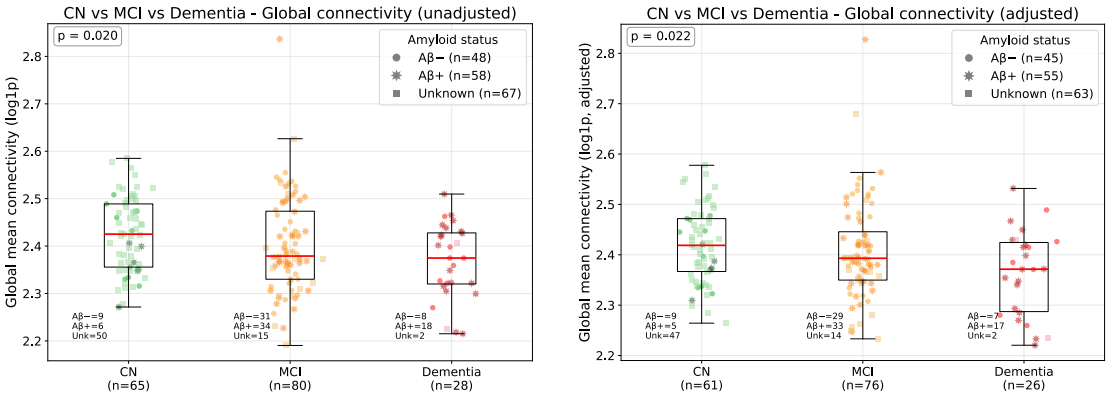


Figure 4.3: Global mean structural connectivity across diagnostic groups before (left) and after (right) adjustment for age, sex, and education. Colors indicate diagnostic group (green: CN, orange: MCI, red: dementia). Marker shapes represent amyloid status: circles correspond to amyloid-negative participants (Aβ-), stars to amyloid-positive participants (Aβ+), and squares to participants with unknown amyloid status. Boxplots summarize the distribution within each group.

In the unadjusted analysis, mean global connectivity appeared slightly lower in the MCI and dementia groups compared with CN participants ($p = 0.020$), although no clear separation between groups was observed. Similar patterns remained after adjustment for covariates ($p = 0.022$), with adjusted connectivity distributions still largely overlapping across groups. Post-hoc Tukey HSD comparisons are reported in Appendix B.2. Pairwise comparisons revealed a significant difference between

CN and dementia participants both before and after covariate adjustment, whereas comparisons involving the MCI group were not statistically significant.

Amyloid status was also displayed for visualization purposes. Amyloid-positive participants were observed across all diagnostic groups, with proportions appearing higher in the MCI and dementia groups compared with CN participants. In the unadjusted dataset, amyloid-positive individuals represented 6/65 participants in the CN group, 34/80 in the MCI group, and 18/28 in the dementia group. However, amyloid status was not formally included as a factor in the statistical models because the present study primarily focused on structural connectivity differences across clinical diagnostic groups. Future studies could investigate the interaction between amyloid burden and structural connectivity alterations in greater detail.

These findings suggest that global structural connectivity remains relatively preserved across diagnostic stages, while disease-related alterations may preferentially affect specific subnetworks rather than the whole connectome uniformly.

4.2.2 Network-Level Connectivity

Network-specific connectivity was then examined for the default mode network (DMN), salience network (SN), and central executive network (CEN).

Default mode network connectivity

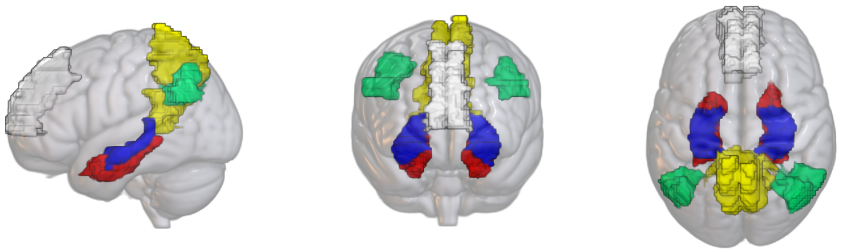


Figure 4.4: Regions included in the DMN based on the AAL atlas. Yellow: medial superior frontal cortex and precuneus; cyan: angular gyrus; blue: hippocampus; red: parahippocampal gyrus; white: posterior cingulate cortex. Lateral, anterior, and superior views are shown from left to right.

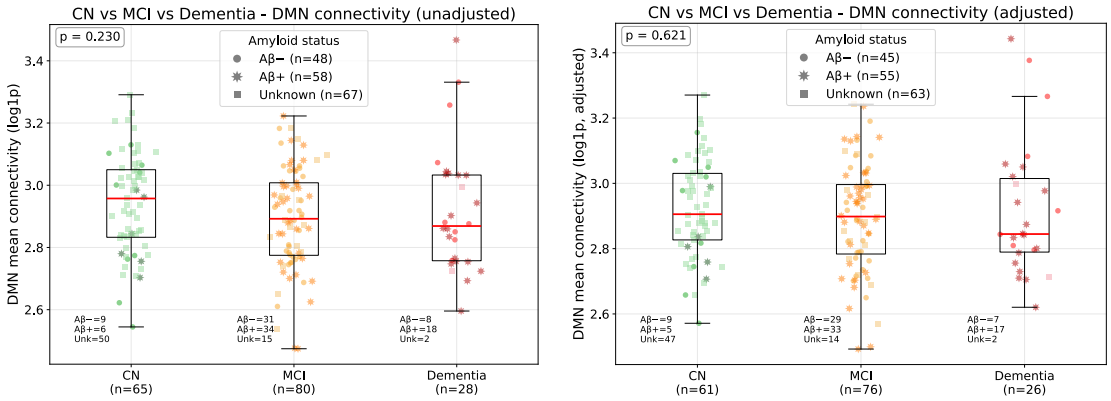


Figure 4.5: Structural connectivity within the DMN across diagnostic groups before (left) and after (right) adjustment for age, sex, and education. Colors indicate diagnostic group (green: CN, orange: MCI, red: dementia). Marker shapes represent amyloid status: circles correspond to amyloid-negative participants (Aβ-), stars to amyloid-positive participants (Aβ+), and squares to participants with unknown amyloid status. Boxplots summarize the distribution within each group.

The anatomical regions included in the DMN are illustrated in Figure 4.4. Structural connectivity within this network across diagnostic groups before and after adjustment for age, sex, and education is presented in Figure 4.5. No statistically significant group effect was observed for DMN connectivity in either the unadjusted ($p = 0.230$) or adjusted analysis ($p = 0.621$). Connectivity distributions largely overlapped between CN, MCI, and dementia participants in both analyses. Post-hoc Tukey HSD comparisons confirmed the absence of significant pairwise differences between diagnostic groups in either analysis (Appendix B.3).

Amyloid-positive participants were observed across all diagnostic categories, without an obvious separation in DMN connectivity values according to amyloid status.

Salience network connectivity

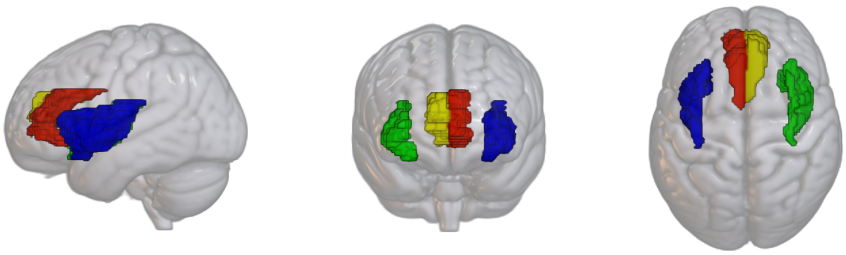


Figure 4.6: Regions included in the SN based on the AAL atlas. Blue and green: insula; yellow and red: anterior cingulate cortex. Lateral, anterior, and superior views are shown from left to right.

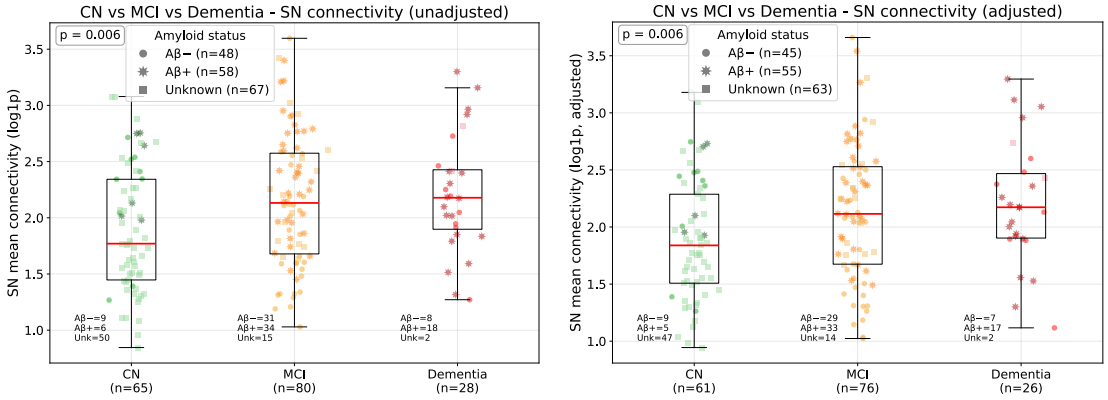


Figure 4.7: Structural connectivity within the SN across diagnostic groups before (left) and after (right) adjustment for age, sex, and education. Colors indicate diagnostic group (green: CN, orange: MCI, red: dementia). Marker shapes represent amyloid status: circles correspond to amyloid-negative participants (Aβ-), stars to amyloid-positive participants (Aβ+), and squares to participants with unknown amyloid status. Boxplots summarize the distribution within each group.

The anatomical regions included in the SN are illustrated in Figure 4.6. Structural connectivity within this network across diagnostic groups is shown in Figure 4.7. In contrast to the DMN, significant differences in SN connectivity were observed between diagnostic groups with $p = 0.006$ in both unadjusted and adjusted analyses.

Mean SN connectivity values tended to be lower in CN participants and higher in MCI and dementia groups. This pattern remained visible after adjustment for age, sex, and education, suggesting that the observed differences were not

solely explained by demographic covariates. Post-hoc Tukey HSD comparisons are reported in Appendix B.4. Significant pairwise differences were observed between CN and MCI participants as well as between CN and dementia participants, whereas no significant difference was detected between the MCI and dementia groups.

Amyloid-positive participants were observed across all diagnostic categories, with proportions appearing higher in the MCI and dementia groups compared with CN participants, similarly to the pattern observed for global connectivity.

Central executive network connectivity

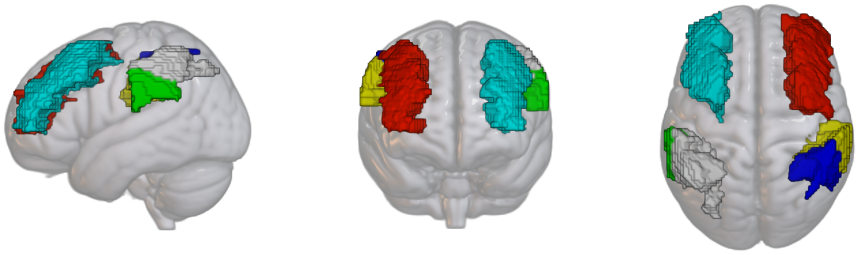


Figure 4.8: Regions included in the CEN based on the AAL atlas. Red and cyan: middle frontal cortex; yellow and white: inferior parietal cortex; blue and green: supramarginal gyrus. Lateral, anterior, and superior views are shown from left to right.

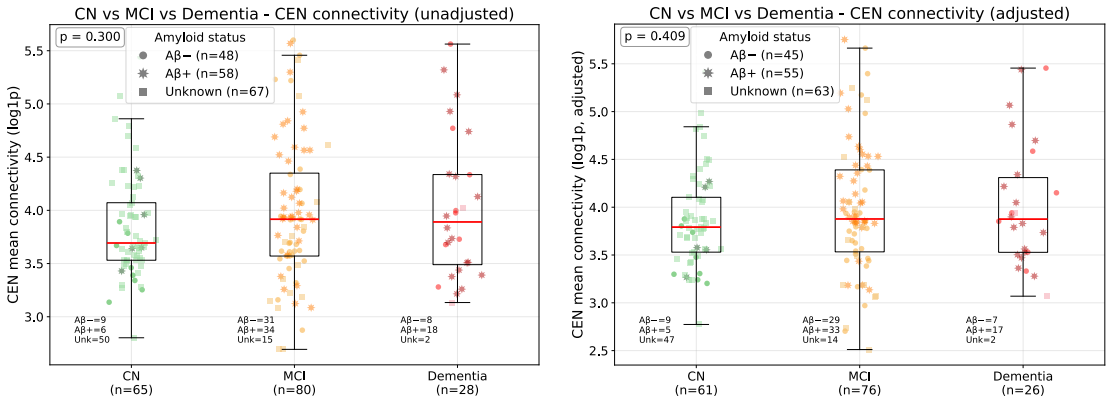


Figure 4.9: Structural connectivity within the CEN across diagnostic groups before (left) and after (right) adjustment for age, sex, and education. Colors indicate diagnostic group (green: CN, orange: MCI, red: dementia). Marker shapes represent amyloid status: circles correspond to amyloid-negative participants (Aβ-), stars to amyloid-positive participants (Aβ+), and squares to participants with unknown amyloid status. Boxplots summarize the distribution within each group.

The anatomical regions included in the CEN are illustrated in Figure 4.8. Figure 4.9 illustrates structural connectivity within this network across diagnostic groups. Connectivity values showed considerable overlap between CN, MCI, and dementia participants in both unadjusted and adjusted analyses with high p-values ($p = 0.300$ and $p = 0.409$, respectively).

Although slightly higher mean CEN connectivity values were observed in MCI and dementia participants, these differences remained modest and highly variable across subjects. Large inter-subject variability was present within all diagnostic categories. Post-hoc Tukey HSD comparisons confirmed the absence of significant pairwise group differences in both unadjusted and adjusted analyses (Appendix B.5).

After adjustment for age, sex, and education, connectivity distributions remained largely unchanged, suggesting limited overall group effects on CEN structural connectivity.

4.2.3 Summary of Findings

Whole-brain structural connectivity did not show major differences between diagnostic groups. At the network level, the DMN and CEN also showed no significant group effects, whereas the SN exhibited significant alterations, even after adjustment for age, sex, and education. More specifically, significant SN differences were primarily driven by lower connectivity values in CN participants compared with both MCI and dementia groups.

4.3 Tract-Based Analysis

A tract-based analysis was performed to identify structural connections associated with cognitive performance across the whole-brain connectome after adjustment for age, sex, and education.

Only edges surviving FDR correction ($q \leq 0.05$), showing positive regression coefficients and a minimum connectivity strength above 10 streamlines were retained. These associations indicate that lower cognitive performance was associated with lower structural connectivity.

For each cognitive score, significant edges were ranked according to their corrected q-values, and the 15 strongest associations were selected for tract extraction and visualization. A summary of the three most significant structural connections

identified for each cognitive score is presented in Table 4.2 (the full table is available in Appendix C). Representative reconstructed tracts are shown in Figure 4.10.

The number of significant connections varied across cognitive domains. Memory showed the lowest number of surviving edges after FDR correction, whereas executive, language, visuospatial, MMSE, and global cognition scores were associated with a larger number of significant pathways (see Table 4.1).

Cognitive score	**Number of significant tracts**
Language composite	84
Global cognitive composite	66
Executive composite	54
Visuospatial composite	24
MMSE	19
Memory composite	5

Table 4.1: Number of significant tracts surviving FDR correction for each cognitive score.

Score	**Edge**	**Region 1**	**Region 2**	**q-value**	**Coefficient**
Executive	(51,50)	Occipital_Mid_L	Occipital_Sup_R	0.0044	0.247
Executive	(47,46)	Lingual_L	Cuneus_R	0.0058	0.217
Executive	(59,50)	Parietal_Sup_L	Occipital_Sup_R	0.0069	0.298
Global cognition	(59,50)	Parietal_Sup_L	Occipital_Sup_R	0.0017	0.313
Global cognition	(89,65)	Temporal_Inf_L	Angular_L	0.0025	0.237
Global cognition	(95,57)	Cerebelum_3_L	Postcentral_L	0.0025	0.232
Language	(89,65)	Temporal_Inf_L	Angular_L	0.0009	0.292
Language	(83,49)	Temporal_Pole_Sup_L	Occipital_Sup_L	0.0022	0.191
Language	(89,11)	Temporal_Inf_L	Frontal_Inf_Oper_L	0.0035	0.215
Memory	(95,57)	Cerebelum_3_L	Postcentral_L	0.0018	0.151
Memory	(83,57)	Temporal_Pole_Sup_L	Postcentral_L	0.0404	0.134
Memory	(105,57)	Cerebelum_9_L	Postcentral_L	0.0431	0.098
MMSE	(51,50)	Occipital_Mid_L	Occipital_Sup_R	0.0007	0.104
MMSE	(60,57)	Parietal_Sup_R	Postcentral_L	0.0079	0.146
MMSE	(68,51)	Precuneus_R	Occipital_Mid_L	0.0090	0.046
Visuospatial	(50,49)	Occipital_Sup_R	Occipital_Sup_L	0.0015	0.156
Visuospatial	(59,44)	Parietal_Sup_L	Calcarine_R	0.0021	0.240
Visuospatial	(51,46)	Occipital_Mid_L	Cuneus_R	0.0031	0.131

Table 4.2: Top significant structural connections associated with cognitive scores after FDR correction.

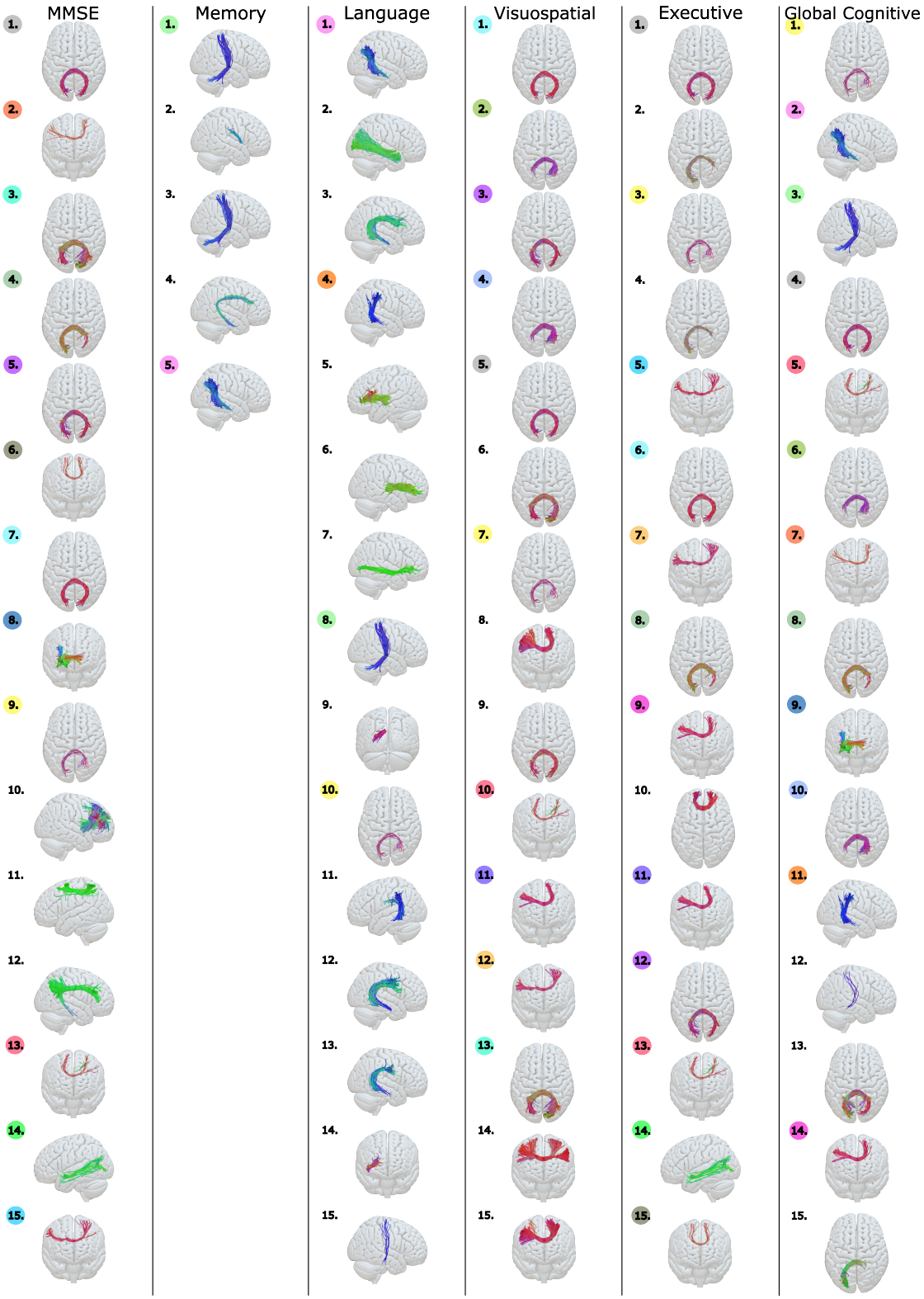


Figure 4.10: Visualization of the most significant white matter tracts associated with cognitive scores after FDR correction. Same colors represent same tracts.

Recurrent Posterior Occipito-Parietal Pathways

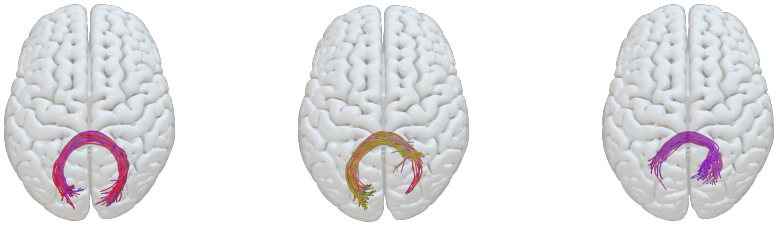


Figure 4.11: Examples of posterior occipito-parietal structural connections identified in the edge-wise analyses.

The most recurrent anatomical pattern involved posterior cortical pathways linking occipital, parietal, precuneus, cuneus, and postcentral regions. These pathways appeared consistently across executive, visuospatial, MMSE, and global cognition analyses. Examples of these tracts are illustrated in Figure 4.11.

Visuospatial analyses showed strong involvement of posterior occipital and parietal pathways, including connections involving the calcarine cortex, cuneus, precuneus, and superior parietal regions. Many of these pathways were interhemispheric, involving communication between posterior regions of both hemispheres.

Global cognition analyses additionally revealed recurrent posterior associative pathways involving the precuneus, superior parietal cortex, occipital regions, and postcentral gyri.

Language-Related Temporo-Frontal and Temporo-Parietal Pathways

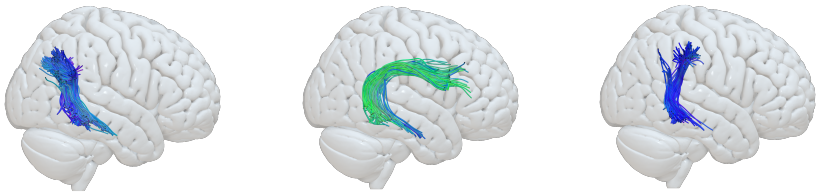


Figure 4.12: Examples of temporo-frontal and temporo-parietal structural connections associated with language performance.

Language-related analyses showed a partially distinct anatomical pattern characterized by recurrent involvement of the inferior temporal gyrus and its connections with frontal, parietal, and sensorimotor regions. Examples of these tracts are shown in Figure 4.12.

These findings suggest the involvement of distributed language-related white matter systems connecting temporal regions with frontal and parietal cortices. Some reconstructed pathways visually resembled long association trajectories linking temporal and frontal regions.

Fronto-Striatal and Subcortical Pathways

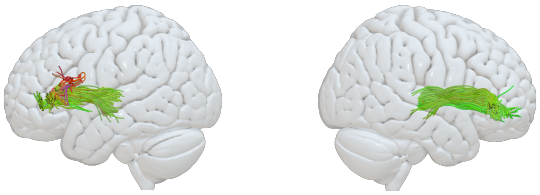


Figure 4.13: Examples of fronto-striatal and subcortical structural connections identified in the edge-wise analyses.

Some significant connections additionally involved subcortical and fronto-striatal regions, as illustrated in Figure 4.13. In particular, language-related analyses identified a strong association between the right caudate nucleus and the right inferior frontal triangular gyrus with a coefficient of 0.461.

Additional subcortical involvement included pathways linking the thalamus with frontal inferior orbital regions. Although less frequent than posterior cortical pathways, these findings suggest that subcortical fronto-striatal systems may also contribute to cognitive and language-related performance.

Limited Memory-Related Connectivity Findings

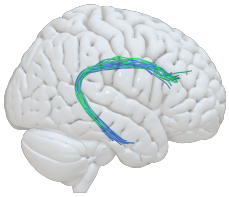


Figure 4.14: Example of a structural connection associated with memory performance.

Compared with the other cognitive domains, memory analyses revealed relatively few significant structural connections after FDR correction.

The identified memory-related pathways mainly involved parahippocampal-cingulate and cerebellar-postcentral connections. In particular, one significant association

linked the left parahippocampal region with the left anterior cingulate cortex, while additional pathways involved cerebellar and postcentral regions (see Figure 4.14).

Unlike executive, visuospatial, MMSE, and global cognition analyses, memory scores did not show widespread distributed posterior connectivity alterations. Instead, memory-related associations appeared more limited and anatomically focal.

Summary of Anatomical Patterns

Overall, similar anatomical connectivity patterns were observed across several cognitive domains. The most recurrent findings involved posterior occipito-parietal and precuneus-related pathways, whereas language-related analyses additionally involved temporo-frontal and temporo-parietal pathways. Memory-related findings were comparatively fewer and more localized.

These recurrent patterns indicate that multiple cognitive domains were associated with partially overlapping large-scale structural connectivity systems.

4.4 Graph-Theoretical Metrics

Graph-theoretical metrics were computed to further characterize alterations in the organization of structural brain networks across diagnostic groups. Group differences between CN, MCI, and dementia participants were assessed using values adjusted for age, sex, and education.

As illustrated in Figure 4.15, significant group differences were observed across all graph-theoretical metrics, with reduced node strength, clustering coefficient, and closeness centrality in MCI and dementia participants. Betweenness centrality, however, tended to increase.

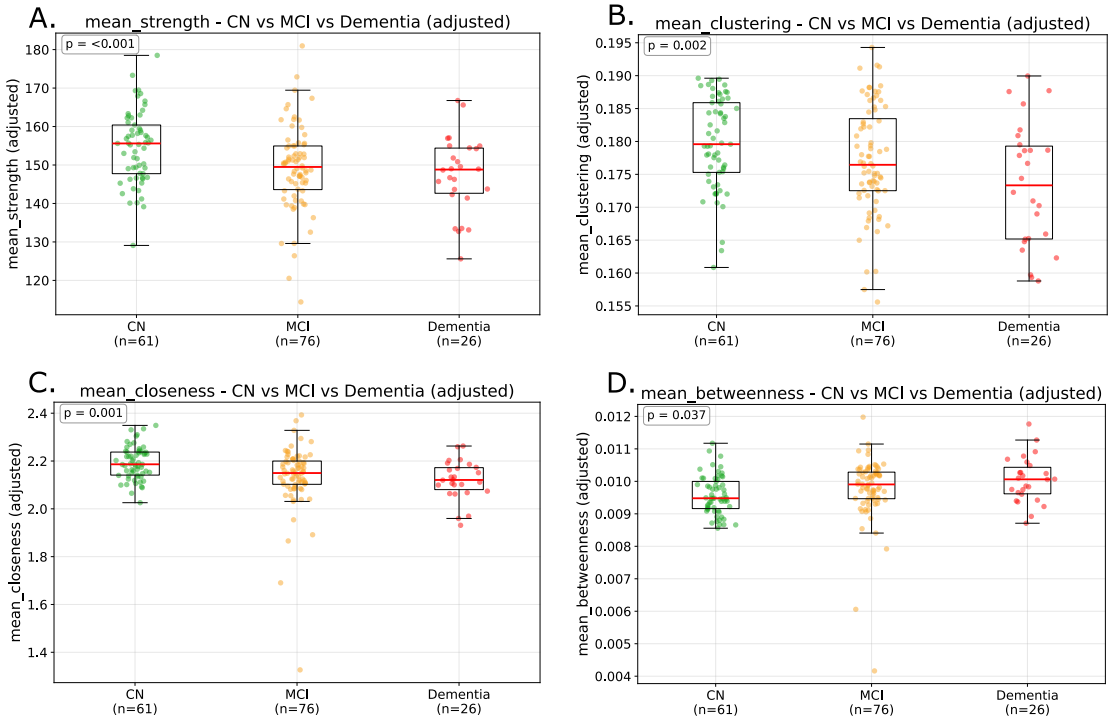


Figure 4.15: Comparison of graph-theoretical metrics across diagnostic groups after adjustment for age, sex, and education. Metrics include mean node strength (A), clustering coefficient (B), closeness centrality (C), and betweenness centrality (D). Green: CN participants, orange: MCI participants, and red: dementia participants. Boxplots summarize the distribution within each group.

Mean node strength showed a strong group effect after covariate adjustment $p < 0.001$. Post-hoc Tukey HSD comparisons revealed significantly higher strength values in CN participants compared with both MCI and dementia participants, whereas no significant difference was observed between MCI and dementia groups (Appendix B.6). These findings suggest a global reduction in structural connectivity strength associated with disease progression.

Similarly, the clustering coefficient differed significantly between groups after adjustment $p = 0.002$. Pairwise comparisons showed a significant reduction in clustering coefficient in dementia participants compared with CN participants, whereas differences involving the MCI group were not statistically significant after adjustment (Appendix B.7). This pattern suggests reduced local network organization in later disease stages.

Closeness centrality also showed a significant group effect $p = 0.001$. Post-hoc analyses demonstrated lower closeness values in both MCI and dementia participants

compared with CN participants, while no significant difference was observed between MCI and dementia groups (Appendix B.8). These results indicate reduced efficiency of information integration across the structural connectome.

In contrast, betweenness centrality exhibited a modest but significant increase across groups after adjustment ($p=0.037$). Post-hoc Tukey HSD comparisons revealed significantly higher betweenness centrality in dementia participants compared with CN participants, whereas comparisons involving the MCI group were not statistically significant (Appendix B.9). This increase may reflect compensatory or reorganizational network processes occurring during disease progression.

Overall, graph-theoretical analyses revealed significant alterations in multiple topological properties of structural brain networks across diagnostic groups, with the most consistent differences observed between CN and dementia participants.

Chapter 5

Discussion

This study investigated alterations in white matter structural connectivity associated with cognitive decline and Alzheimer's disease using diffusion MRI, tractography, and connectome-based analyses. The results showed some significant changes in global and network-level structural connectivity, as well as associations between white matter connections and cognitive performance. The present chapter discusses these findings in relation to previous literature and current knowledge of Alzheimer's disease as a large-scale network disorder. Methodological limitations are also discussed in this chapter.

5.1 Results Interpretation

5.1.1 Global and Network-Level Connectivity Findings

At the global level, structural connectivity showed a slight but significant decrease in dementia participants compared with CN subjects. Although the differences between groups were relatively small and connectivity values partially overlapped, the observed decrease in global connectivity suggests that cognitive decline is associated with progressive alterations of structural brain connections.

The relatively limited magnitude of global connectivity differences may indicate that neurodegenerative processes do not initially produce homogeneous disruption of the entire structural network. Instead, structural alterations may preferentially affect specific pathways or networks while other parts of the connectome remain relatively preserved. This interpretation is consistent with the current view of

Alzheimer's disease as a network-based disorder affecting specific large-scale brain systems.[43, 69]

At the network level, distinct patterns of connectivity alterations were observed across the investigated networks, suggesting that neurodegeneration affects specific cognitive systems differently.

Within the DMN, although a tendency toward lower connectivity was visible in dementia participants, no statistically significant differences in structural connectivity were observed between diagnostic groups. The DMN is strongly implicated in episodic memory and is known to be particularly vulnerable in Alzheimer's disease.[12, 14] Functional MRI studies have consistently demonstrated DMN dysfunction in Alzheimer's disease, especially involving posterior cingulate and precuneus regions.[14, 70] The absence of significant structural differences in the DMN may suggest that structural alterations in this network are still limited or remain difficult to detect in the studied cohort.

In contrast, the SN showed significant connectivity differences between groups, even after adjustment for age, sex, and education. Interestingly, SN connectivity tended to increase in MCI and dementia participants compared with CN subjects. Although neurodegenerative diseases are often associated with reduced connectivity, increased connectivity within specific networks has previously been reported in early or intermediate disease stages and may reflect compensatory mechanisms or network reorganization.[15, 71, 72] The SN plays a central role in attentional control and communication between major cognitive networks, particularly between the DMN and executive networks.[15] Increased SN connectivity may therefore represent an adaptive response attempting to maintain cognitive performance despite progressive disruption of other large-scale networks.

Regarding the CEN, no clear group differences were identified. Structural connectivity within this network remained relatively stable across diagnostic categories. This apparent preservation of CEN structural organization may suggest that executive-related structural pathways are less severely affected in the studied population or that structural executive network alterations emerge later during disease progression.

Interestingly, the combination of mildly reduced global connectivity, relatively preserved DMN and CEN structural organization, and increased SN connectivity may support the hypothesis that early neurodegenerative processes involve selective network reorganization rather than uniform structural collapse. These findings are compatible with the idea that some networks may transiently compensate for dysfunction occurring in other cognitive systems before more widespread disconnection

develops.[69]

Overall, these results highlight the importance of investigating structural connectivity at the network level in addition to whole-brain analyses. While global measures provide information about overall connectome integrity, network-specific analyses may better capture the selective vulnerability and adaptive reorganization processes associated with cognitive decline and neurodegeneration.

5.1.2 Tract-Based Analyses

The tract-based analyses showed significant associations between several white matter connectivity pathways and cognitive performance across several cognitive domains. In general, lower cognitive scores were associated with lower connectivity in multiple white matter tracts. These findings suggest that cognitive decline in Alzheimer's disease is related to widespread alterations of brain connectivity rather than damage restricted to a single tract.

After visualization of the significant tracts in Figure 4.10, several connections appeared to share similar anatomical trajectories. These tracts were therefore grouped to facilitate interpretation.

(a) Posterior interhemispheric and visuo-parietal pathways

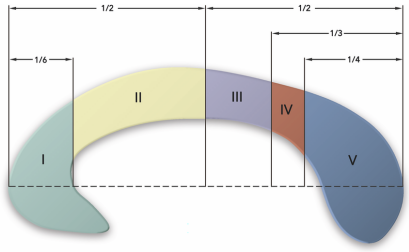
Composite score	Associated tracts
MMSE	1, 3, 4, 5, 7, 9, 13
Visuospatial	1, 2, 3, 4, 5, 6, 7, 9, 10, 13
Executive	1, 2, 3, 4, 6, 8, 12, 13
Global cognition	1, 4, 5, 6, 8, 10, 13, 15

Table 5.1: Tracts associated with posterior interhemispheric and visuo-parietal pathways. Numbers correspond to tract labels shown in Figure 4.10 in the Results section.

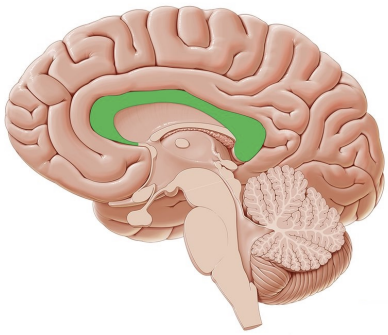
A major finding of the tract-based analysis was the recurrent involvement of posterior cortical and interhemispheric pathways. Visual inspection of the reconstructed streamlines showed recurrent connections involving occipital, precuneus, superior parietal, cuneus, lingual, and postcentral regions. These pathways appeared consistently across visuospatial, executive, MMSE, and global cognitive scores.

Many of these posterior interhemispheric connections appeared anatomically compatible with fibers passing through the posterior part of the corpus callosum, particularly the splenium, as illustrated in Figure 5.1. This tract may therefore

correspond to the forceps major. This pathway connects posterior occipital regions between the two hemispheres and is involved in visual information processing. The frequent association of these tracts with visuospatial scores is consistent with the role of posterior brain regions in visuospatial and attentional functions.[26]



(a) Corpus callosum divided into five regions: I. Rostrum/Genu, II. Anterior Midbody, III. Posterior Midbody, IV. Isthmus and V. Splenium.[73]



(b) Sagittal view of the entire corpus callosum.[74]

Figure 5.1: Corpus callosum anatomy.

Many of these recurrent posterior pathways also involved the precuneus and superior parietal regions across multiple cognitive domains. The precuneus is a highly connected associative region involved in visuospatial processing, attention, and integration of information from multiple brain regions.[75, 76] Its recurrent involvement in the present analyses suggests that altered posterior connectivity may contribute not only to visuospatial dysfunction, but also to broader cognitive impairment.

These findings support the idea that cognitive impairment is associated with alterations in distributed posterior associative networks rather than isolated focal lesions. The repeated involvement of posterior occipital, parietal, and precuneus pathways may reflect altered communication between visual and attentional regions.

(b) Language-related temporo-frontal and temporo-parietal pathways

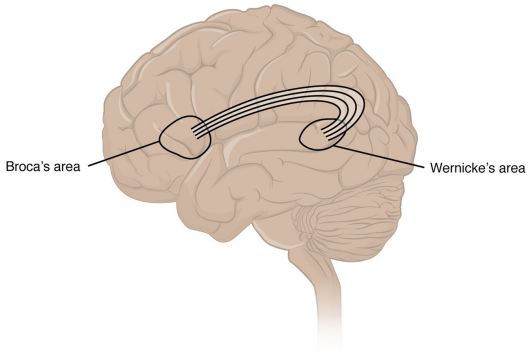
Composite score	Associated tracts
Language	1, 3, 4, 11, 12, 13, 15
Global cognition	2, 11
Memory	5

Table 5.2: Tracts associated with language-related temporo-frontal and temporo-parietal pathways. Numbers correspond to tract labels shown in Figure 4.10 in the Results section.

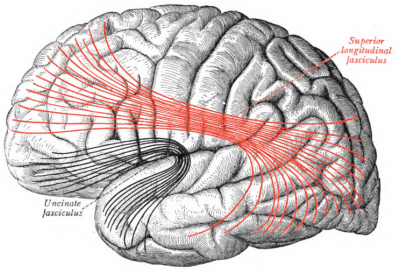
A second major anatomical pattern involved temporo-frontal and temporo-parietal pathways, particularly around the left inferior temporal gyrus and its connections with frontal and parietal regions. These pathways were frequently observed in the language composite.

This organization is compatible with known language networks involving posterior temporal and parietal language-related regions traditionally associated with Wernicke's area, as well as inferior frontal regions associated with Broca's area.[77] Some reconstructed streamlines visually resembled long association fibers linking temporal and frontal cortices and may partially overlap with pathways such as the arcuate fasciculus or parts of the superior longitudinal fasciculus, which are illustrated in Figure 5.2.[78, 79] However, these anatomical interpretations should be considered approximate because the analysis was based on atlas-defined regions.

Overall, the recurrent involvement of temporo-frontal and temporo-parietal pathways in the language composite is consistent with the known anatomical organization of large-scale language networks.[78, 79]



(a) Arcuate fasciculus linking posterior temporal and inferior frontal language-related regions.[80]



(b) Superior longitudinal fasciculus.[81]

Figure 5.2: Language-related anatomical tracts.

(c) Fronto-striatal and subcortical pathways

Composite score	Associated tracts
Language	5

Table 5.3: Tract associated with fronto-striatal and subcortical pathways. Numbers correspond to tract labels shown in Figure 4.10 in the Results section.

Another interesting connection identified involved the strong correlation (0.461) between the right caudate nucleus and the right inferior frontal triangular gyrus in the language composite. This finding suggests that language performance may not rely exclusively on cortical fronto-temporal systems, but may also involve subcortical fronto-striatal circuits.

Subcortical structures such as the caudate nucleus and thalamus are known to contribute to executive aspects of language processing, including cognitive control and speech regulation. These findings may indicate that executive control processes also contribute to language performance.[77]

(d) Sensorimotor and fronto-parietal pathways

Composite score	Associated tracts
Executive	5, 7, 9, 11, 15
MMSE	2, 6, 15
Visuospatial	8, 11, 12, 14, 15
Global cognition	7, 14

Table 5.4: Tracts associated with sensorimotor and fronto-parietal pathways. Numbers correspond to tract labels shown in Figure 4.10 in the Results section.

Several significant tracts involved precentral, postcentral, supplementary motor, paracentral, supramarginal, and superior parietal regions. These pathways were identified across executive, visuospatial, MMSE, and global cognition analyses.

Visual inspection of the reconstructed streamlines suggested that many of these pathways followed interhemispheric or fronto-parietal associative trajectories. Several streamlines connected sensorimotor regions between hemispheres through trajectories compatible with transcallosal fibers. Based on their anatomical course, some of these pathways may involve callosal regions corresponding to the anterior or posterior midbody of the corpus callosum (Figure 5.1), which are known to contain sensorimotor interhemispheric fibers.[82]

The regions involved in these pathways are known to participate in visuomotor coordination, somatosensory integration, spatial attention, and motor planning. Disruption of these pathways may indirectly contribute to cognitive dysfunction by affecting communication between frontal, parietal, and sensorimotor regions.[83]

(e) Cingulum and memory-related pathways

Composite score	Associated tracts
Memory	4
MMSE	12

Table 5.5: Tracts associated with limbic and memory-related pathways. Numbers correspond to tract labels shown in Figure 4.10 in the Results section.

Memory-related analyses showed fewer significant connections than the other cognitive domains. Nevertheless, one particularly relevant pathway was identified between the left parahippocampal region and the left anterior cingulate cortex. Visual inspection of the reconstructed streamlines suggested an anatomical trajectory compatible with the cingulum bundle, a major limbic association pathway linking medial temporal, cingulate, and frontal regions.

The cingulum, illustrated in Figure 5.3, plays a major role in episodic memory and cognitive control by connecting medial temporal structures involved in memory processing with cingulate and prefrontal regions associated with attention, executive regulation, and emotional integration.[84, 85]

The presence of a cingulum-related pathway in the memory analyses is consistent with the known involvement of medial temporal and limbic regions in Alzheimer's disease.[26, 85]

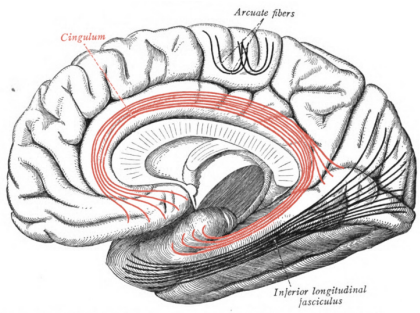


Figure 5.3: Cingulum bundle connecting medial temporal, cingulate, and frontal regions.[86]

Overall interpretation

Taken together, the tract-based results suggest that cognitive decline is associated with alterations in several major white matter systems rather than a single isolated pathway. The most recurrent patterns involved posterior interhemispheric and visuo-parietal pathways, temporo-frontal and temporo-parietal language-related

connections, sensorimotor-related tracts, and a memory-relevant cingulum-related connection.

These findings suggest that cognitive impairment involves alterations in distributed posterior brain networks rather than isolated lesions. The presence of similar pathways across several cognitive scores suggests that some white matter tracts may contribute to multiple cognitive functions.

5.1.3 Graph-Theoretical Analyses

Graph-theoretical analyses were performed to investigate alterations in large-scale structural network organization beyond simple connectivity strength measures. Several graph metrics were examined, including node strength, clustering coefficient, closeness centrality, and betweenness centrality.

Overall, significant differences were observed between diagnostic groups for the four metrics. Mean node strength, clustering coefficient, and closeness centrality were reduced in dementia patients compared with CN subjects. In contrast, betweenness centrality showed a slight increase in dementia. In most cases, MCI subjects presented intermediate values between CN and dementia groups, suggesting progressive network alterations along the cognitive decline continuum.

The reduction in mean node strength suggests a global decrease in structural connectivity across the brain network. Since node strength reflects the sum of connection weights linked to each node, lower values may indicate widespread white matter disconnection and reduced overall communication capacity within the structural connectome. [87–89]

Similarly, the observed decrease in clustering coefficient may reflect disruption of local network organization. Clustering coefficient quantifies the tendency of neighboring nodes to remain interconnected and is therefore considered a marker of local segregation and network specialization. Reduced clustering may indicate a loss of efficient local processing and reduced structural organization of neighboring brain regions. [87–89]

Closeness centrality was also significantly reduced in dementia patients. Because closeness centrality reflects how efficiently a node can communicate with the rest of the network through short paths, lower values may suggest decreased global communication efficiency and impaired large-scale integration of information across the connectome. [88]

In contrast, betweenness centrality showed a slight increase in dementia patients. Betweenness centrality reflects the proportion of shortest paths passing through a node and is often interpreted as a measure of hubness. Increased betweenness may therefore indicate that communication becomes concentrated through fewer remaining pathways or hub regions as structural connectivity deteriorates. This pattern could reflect network reorganization or compensatory redistribution of information flow in response to progressive structural disconnection. [88, 89]

Taken together, these results suggest that cognitive decline is associated with widespread alterations in structural brain networks. Together, these findings suggest reduced network efficiency and altered organization of communication pathways in dementia.

5.2 Limitations and Methodological Considerations

Several methodological considerations and limitations should be taken into account when interpreting the results of the present study.

First, the study relied on diffusion MRI tractography and SIFT2-weighted structural connectivity matrices to estimate white matter organization. Although these methods provide valuable information regarding structural brain connectivity, they remain indirect estimations of anatomical pathways. Reconstructed streamlines do not correspond directly to true anatomical axons and may therefore include both false-positive and false-negative connections. While modern tractography approaches and SIFT2 weighting improve the biological plausibility of connectivity estimates, some degree of reconstruction uncertainty remains unavoidable.

Second, structural connectivity matrices were constructed using the AAL atlas for brain parcellation. Atlas-based approaches facilitate reproducibility and group-level comparisons but also introduce limitations related to predefined anatomical boundaries and limited spatial resolution. Different atlases or finer parcellation schemes may reveal additional connectivity alterations that were not captured in the present analyses.

Because edge-wise analyses involve a very large number of statistical comparisons, FDR correction using the Benjamini–Hochberg procedure was applied to reduce the risk of false-positive findings. However, this correction may also decrease sensitivity to weaker but biologically meaningful effects.

Several limitations related to the study cohort should also be considered. The sample size remained relatively limited, particularly for the dementia group, resulting in imbalance between diagnostic categories. This may have reduced statistical power and limited the ability to detect more subtle connectivity alterations. In addition, missing data for some cognitive scores reduced the number of participants available for specific analyses.

Another limitation concerns tract extraction and anatomical interpretation. Significant tracts were visualized in a single representative subject to facilitate anatomical interpretation. However, this approach does not fully capture inter-subject anatomical variability. Furthermore, the identification of specific white matter bundles from atlas-defined endpoints remains approximate, since tractography provides only an indirect reconstruction of white matter anatomy.

The cross-sectional design of the study also limits conclusions regarding the temporal evolution of connectivity alterations. Longitudinal analyses would be necessary to determine whether the observed structural changes precede cognitive decline or reflect later stages of disease progression.

Finally, only structural connectivity was investigated in the present work. Combining diffusion MRI with additional modalities such as functional MRI, PET biomarkers, or longitudinal cognitive assessments could provide a more comprehensive understanding of neurodegenerative processes associated with Alzheimer's disease.

Conclusion

This study investigated structural connectivity alterations associated with cognitive decline and Alzheimer's disease using advanced diffusion MRI tractography, connectome analyses, and graph-theoretical approaches. By combining probabilistic tractography, SIFT2-weighted connectivity matrices, and edge-wise statistical analyses, this work aimed to characterize how neurodegeneration affects large-scale white matter organization and communication between brain regions.

The results revealed several connectivity alterations across the Alzheimer's disease spectrum. While global structural connectivity showed only modest differences between diagnostic groups, significant changes were observed at more specific levels of analysis. At the network level, the salience network exhibited significant connectivity differences between groups, whereas the default mode and central executive networks remained relatively preserved. Edge-wise analyses identified multiple structural connections associated with cognitive performance, particularly involving posterior occipito-parietal pathways as well as temporo-frontal and temporo-parietal regions. In addition, graph-theoretical analyses revealed significant alterations in network topology, including reduced node strength, clustering coefficient, and closeness centrality, together with increased betweenness centrality in cognitively impaired participants.

These findings support the hypothesis that Alzheimer's disease is associated with progressive alterations of structural brain networks that may not always be detectable through global connectivity measures alone. Instead, disease-related changes appear to affect specific subnetworks, individual structural connections, and topological properties of the connectome.

Several limitations of the present study should nevertheless be considered. Tractography remains an indirect reconstruction of white matter pathways and is influenced by methodological choices such as atlas selection, tractography parameters, and network construction strategies. In addition, the cross-sectional design of the study does not allow direct assessment of disease progression over time. Future

longitudinal studies combining structural connectivity with other imaging and biomarker modalities could provide a more comprehensive understanding of the mechanisms underlying cognitive decline.

Overall, this work highlights the value of structural connectomics for investigating brain network alterations associated with Alzheimer's disease. Advanced diffusion MRI techniques and connectome-based analyses provide complementary information to traditional neuroimaging approaches and may contribute to the development of imaging biomarkers for the characterization and monitoring of neurodegenerative disorders.

Bibliography

[1] Fondation pour la Recherche Médicale. "Tout savoir sur la maladie d'alzheimer. "[Online]. Available: https://www.frm.org/fr/maladies/recherches-maladies-neurologiques/maladies-d-alzheimer/focus-maladie-d-alzheimer.

[2] P. Mespouille, *Alzheimer, Parkinson, Charcot... Quand les neurones ne répondent plus*. Mardaga, 2022.

[3] J. A. Hardy and G. A. Higgins, "Alzheimer's disease: the amyloid cascade hypothesis," *Science*, vol. 256, no. 5054, pp. 184–185, 1992. DOI: 10.1126/science.1566067.

[4] D. J. Selkoe and J. Hardy, "The amyloid hypothesis of alzheimer's disease at 25 years," *EMBO Molecular Medicine*, vol. 8, no. 6, pp. 595–608, 2016. DOI: 10.15252/emmm.201606210.

[5] C. E. Sexton, U. G. Kalu, N. Filippini, C. E. Mackay, and K. P. Ebmeier, "A meta-analysis of diffusion tensor imaging in mild cognitive impairment and alzheimer's disease," *Neurobiology of Aging*, vol. 32, no. 12, 2322.e5–2322.e18, 2011. DOI: 10.1016/j.neurobiolaging.2010.05.019.

[6] G.-f. Chen *et al.*, "Amyloid beta: Structure, biology and structure-based therapeutic development," *Acta Pharmacologica Sinica*, vol. 38, no. 9, pp. 1205–1235, 2017. DOI: 10.1038/aps.2017.28.

[7] G. S. Bloom, "Amyloid-β and tau: the trigger and bullet in Alzheimer disease pathogenesis," *JAMA Neurology*, vol. 71, no. 4, pp. 505–508, 2014. DOI: 10.1001/jamaneurol.2013.5847.

[8] D. F. V. Pîrşcoveanu *et al.*, "Tau protein in neurodegenerative diseases – a review," *Romanian Journal of Morphology and Embryology*, vol. 58, no. 4, pp. 1141–1150, 2017. [Online]. Available: https://pubmed.ncbi.nlm.nih.gov/29556602/.

[9] V. R. Bitra, S. R. Challa, P. C. Adiukwu, and D. Rapaka, "Tau trajectory in alzheimer's disease: Evidence from the connectome-based computational models," *Brain Research Bulletin*, vol. 203, p. 110 777, 2023. DOI: 10.1016/j.brainresbull.2023.110777.

[10] R. L. Landry and M. E. Embers, "Does dementia have a microbial cause?" *NeuroSci*, vol. 3, pp. 262–283, 2022. DOI: 10.3390/neurosci3020019.

[11] R. A. Sperling *et al.*, "Toward defining the preclinical stages of Alzheimer's disease: recommendations from the National Institute on Aging-Alzheimer's Association workgroups on diagnostic guidelines for Alzheimer's disease," *Alzheimer's & Dementia*, vol. 7, no. 3, pp. 280–292, 2011. DOI: 10.1016/j.jalz.2011.03.003.

[12] W. Jagust, "Imaging the evolution and pathophysiology of alzheimer disease," *Nature Reviews Neuroscience*, vol. 19, no. 11, pp. 687–700, 2018. DOI: 10.1038/s41583-018-0067-3.

[13] D. van der Linden, M. Tops, and A. B. Bakker, "Go with the flow: A neuroscientific view on being fully engaged," *European Journal of Neuroscience*, vol. 53, no. 4, pp. 947–963, 2021. DOI: 10.1111/ejn.15014.

[14] M. Weiler, B. Machado de Campos, M. H. Nogueira, B. P. Damasceno, F. Cendes, and M. L. F. Balthazar, "Structural connectivity of the default mode network and cognition in alzheimer's disease," *Psychiatry Research: Neuroimaging*, vol. 223, pp. 15–22, 2014. DOI: 10.1016/j.pscychresns.2014.04.008.

[15] Q. Yuan *et al.*, "Functional changes in the salience network of patients with Alzheimer's disease," *Brain and Behavior*, 2023. DOI: 10.1002/brb3.3169.

[16] X. He *et al.*, "Abnormal salience network in normal aging and in amnestic mild cognitive impairment and alzheimer's disease," *Human Brain Mapping*, vol. 35, no. 7, pp. 3446–3464, 2014. DOI: 10.1002/hbm.22414.

[17] K. M. Daigle, M. O. Pietrzykowski, A. B. Waters, L. P. Swenson, and D. A. Gansler, "Central executive network and executive function in patients with alzheimer's disease and healthy individuals: Meta-analysis of structural and functional mri," *The Journal of Neuropsychiatry and Clinical Neurosciences*, vol. 34, no. 3, pp. 204–213, 2022. DOI: 10.1176/appi.neuropsych.20110279.

[18] R. D. Fields, "White matter in learning, cognition and psychiatric disorders," *Trends in Neurosciences*, vol. 31, no. 7, pp. 361–370, 2008. DOI: 10.1016/j.tins.2008.04.001.

[19] G. Bartzokis, "Age-related myelin breakdown: A developmental model of cognitive decline and alzheimer's disease," *Neurobiology of Aging*, vol. 25, no. 1, pp. 5–18, 2004. DOI: 10.1016/j.neurobiolaging.2003.03.001.

[20] A. V. Avram, "Diffusion tensor imaging of myelin water," PhD thesis, National Institutes of Health, 2011. DOI: 10.13140/RG.2.2.21412.88965.

[21] M. Catani and M. Thiebaut de Schotten, "A diffusion tensor imaging tractography atlas for virtual in vivo dissections," *Cortex*, vol. 44, no. 8, pp. 1105–1132, 2008. DOI: 10.1016/j.cortex.2008.05.004.

[22] X. Delbeuck, M. Van der Linden, and F. Collette, "Alzheimer's disease as a disconnection syndrome?" *Neuropsychology Review*, vol. 13, no. 2, pp. 79–92, 2003. DOI: 10.1023/a:1023832305702.

[23] R. D. Fields, "A new mechanism of nervous system plasticity: Activity-dependent myelination," *Nature Reviews Neuroscience*, vol. 16, pp. 756–767, 2015. DOI: 10.1038/nrn4023.

[24] M. Bradl and H. Lassmann, "Oligodendrocytes: Biology and pathology," *Acta Neuropathologica*, vol. 119, pp. 37–53, 2010. DOI: 10.1007/s00401-009-0601-5.

[25] L. Pantoni, "Cerebral small vessel disease: From pathogenesis and clinical characteristics to therapeutic challenges," *The Lancet Neurology*, vol. 9, no. 7, pp. 689–701, 2010. DOI: 10.1016/S1474-4422(10)70104-6.

[26] C. Luo *et al.*, "White matter microstructural damage as an early sign of subjective cognitive decline," *Frontiers in Aging Neuroscience*, vol. 11, p. 378, 2020. DOI: 10.3389/fnagi.2019.00378.

[27] Y. Chen, Y. Wang, Z. Song, Y. Fan, T. Gao, and X. Tang, "Abnormal white matter changes in alzheimer's disease based on diffusion tensor imaging: A systematic review," *Ageing Research Reviews*, vol. 87, p. 101 911, 2023. DOI: 10.1016/j.arr.2023.101911.

[28] O. Sporns, *Networks of the Brain*. MIT Press, 2010, ISBN: 9780262014694. DOI: 10.7551/mitpress/8476.001.0001.

[29] A. J. Alghamdi, "The value of various post-processing modalities of diffusion weighted imaging in the detection of multiple sclerosis," *Brain Sciences*, vol. 13, no. 4, p. 622, 2023. DOI: 10.3390/brainsci13040622.

[30] J. L. Wisnowski, R. C. Ceschin, and V. J. Schmidthorst. "Diffusion-weighted magnetic resonance imaging: Principles and implementation in clinical and research settings. "[Online]. Available: https://clinicalgate.com/diffusion-weighted-magnetic-resonance-imaging-principles-and-implementation-in-clinical-and-research-settings/.

[31] A. Ghosh and R. Deriche, "From diffusion mri to brain connectomics," in *Modeling in Computational Biology and Biomedicine*, F. Cazals and P. Kornprobst, Eds., Berlin, Heidelberg: Springer, 2013, pp. 193–234. DOI: 10.1007/978-3-642-31208-3_6.

[32] F. Dell'Acqua, M. Descoteaux, and A. Leemans, Eds., *Handbook of Diffusion MR Tractography: Imaging Methods, Biophysical Models, Algorithms and Applications*. Academic Press, 2020.

[33] V. G. Kiselev, "Fundamentals of diffusion mri physics," *NMR in Biomedicine*, vol. 30, no. 3, e3602, 2017. DOI: 10.1002/nbm.3602.

[34] "Dti processing - voxel-based versus tract-based diffusion imaging," Accessed: Mar. 9, 2026. [Online]. Available: https://www.diffusion-imaging.com/2012/10/voxel-based-versus-track-based.html.

[35] B. Jeurissen, J.-D. Tournier, T. Dhollander, A. Connelly, and J. Sijbers, "Multi-tissue constrained spherical deconvolution for improved analysis of multi-shell diffusion mri data," *NeuroImage*, vol. 103, pp. 411–426, 2014. DOI: 10.1016/j.neuroimage.2014.07.061.

[36] Y. Saito *et al.*, "Early psychosis is characterized by white matter abnormalities in fiber structures supporting local connectivity," *medRxiv*, 2025, Preprint, version 1, posted 14 May 2025. DOI: 10.1101/2025.05.13.25327498.

[37] Y. Shuai *et al.*, "Deterministic versus probabilistic tractography: Impact on white matter bundle shape," *bioRxiv*, 2025. DOI: 10.1101/2025.08.19.669949.

[38] F. Calamante, "The seven deadly sins of measuring brain structural connectivity using diffusion mri streamlines fibre-tracking," *Diagnostics*, vol. 9, no. 3, p. 115, 2019. DOI: 10.3390/diagnostics9030115.

[39] D. K. Jones, "Studying connections in the living human brain with diffusion mri," *Cortex*, vol. 44, no. 8, pp. 936–952, 2008. DOI: 10.1016/j.cortex.2008.05.002.

[40] K. G. Schilling *et al.*, "Limits to anatomical accuracy of diffusion tractography using modern approaches," *NeuroImage*, vol. 185, pp. 1–11, 2019. DOI: 10.1016/j.neuroimage.2018.10.029.

[41] R. E. Smith, J.-D. Tournier, F. Calamante, and A. Connelly, "Sift: Spherical-deconvolution informed filtering of tractograms," *NeuroImage*, vol. 67, pp. 298–312, 2013. DOI: 10.1016/j.neuroimage.2012.11.049.

[42] R. E. Smith, J.-D. Tournier, F. Calamante, and A. Connelly, "Sift2: Enabling dense quantitative assessment of brain white matter connectivity using streamlines tractography," *NeuroImage*, vol. 119, pp. 338–351, 2015. DOI: 10.1016/j.neuroimage.2015.06.092.

[43] W. Liu *et al.*, "The whole-brain structural and functional connectome in alzheimer's disease spectrum: A multimodal bayesian meta-analysis of graph theoretical characteristics," *Neuroscience & Biobehavioral Reviews*, vol. 174, 2025. DOI: 10.1016/j.neubiorev.2025.106174.

[44] Z. Dai *et al.*, "Disrupted structural and functional brain networks in Alzheimer's disease," *Neurobiology of Aging*, vol. 75, pp. 71–82, 2019. DOI: 10.1016/j.neurobiolaging.2018.11.005.

[45] M. Rubinov and O. Sporns, "Complex network measures of brain connectivity: Uses and interpretations," *NeuroImage*, vol. 52, no. 3, pp. 1059–1069, 2010. DOI: 10.1016/j.neuroimage.2009.10.003.

[46] M. Guye, G. Bettus, F. Bartolomei, and P. J. Cozzone, "Graph theoretical analysis of structural and functional connectivity mri in normal and pathological brain networks," *Magnetic Resonance Materials in Physics, Biology and Medicine*, vol. 23, no. 5–6, pp. 409–421, 2010. DOI: 10.1007/s10334-010-0205-z.

[47] I. Stepan-Buksakowska *et al.*, "Diffusion tensor imaging in Alzheimer disease and mild cognitive impairment," *Neurologia i Neurochirurgia Polska*, vol. 46, no. 5, pp. 462–471, 2012. DOI: 10.5114/ninp.2012.31357.

[48] Henry Gray. "Gray751 - superior longitudinal fasciculus." Illustration from Gray's Anatomy, Accessed: Mar. 10, 2026. [Online]. Available: https://fr.wikipedia.org/wiki/Fichier:Gray751_-_Superior_longitudinal_fasciculus.png.

[49] M. Daianu *et al.*, "Breakdown of brain connectivity between normal aging and alzheimer's disease: A structural k-core network analysis," *Brain Connectivity*, vol. 3, no. 4, pp. 407–422, 2013. DOI: 10.1089/brain.2012.0137.

[50] G. Prasad, S. H. Joshi, T. M. Nir, A. W. Toga, and P. M. Thompson, "Brain connectivity and novel network measures for alzheimer's disease classification," *Neurobiology of Aging*, vol. 36, no. Supplement 1, S121–S131, 2015. DOI: 10.1016/j.neurobiolaging.2014.04.037.

[51] C.-Y. Lo, P.-N. Wang, K.-H. Chou, J. Wang, Y. He, and C.-P. Lin, "Diffusion tensor tractography reveals abnormal topological organization in structural cortical networks in Alzheimer's disease," *The Journal of Neuroscience*, vol. 30, no. 50, pp. 16 876–16 885, 2010. DOI: 10.1523/JNEUROSCI.4136-10.2010.

[52] Y. D. Reijmer, A. Leemans, K. Caeyenberghs, S. M. Heringa, H. L. Koek, and G. J. Biessels, "Disruption of cerebral networks and cognitive impairment in alzheimer disease," *Neurology*, vol. 80, no. 15, pp. 1370–1377, 2013. DOI: 10.1212/WNL.0b013e31828c2ee5.

[53] M. Lv *et al.*, "Analysis of advanced diffusion models assessing white matter microstructure in alzheimer's disease," *Scientific Reports*, vol. 15, p. 26 266, 2025. DOI: 10.1038/s41598-025-09412-1.

[54] E. Developers, *Elikopy documentation*, https://elikopy.readthedocs.io/en/latest/introduction.html, Accessed: 2026-05-22, 2024.

[55] Q. Dessain, M. Simon, and N. Delinte, *ElikoPy*, https://github.com/Hyedryn/elikopy, GitHub repository, version v0.4.4, accessed 31 May 2026, 2024.

[56] N. Otsu, "A threshold selection method from gray-level histograms," *IEEE Transactions on Systems, Man, and Cybernetics*, vol. 9, no. 1, pp. 62–66, 1979. DOI: 10.1109/TSMC.1979.4310076.

[57] J. Veraart, D. S. Novikov, D. Christiaens, B. Ades-Aron, J. Sijbers, and E. Fieremans, "Denoising of diffusion mri using random matrix theory," *NeuroImage*, vol. 142, pp. 394–406, Nov. 2016. DOI: 10.1016/j.neuroimage.2016.08.016.

[58] J. L. R. Andersson and S. N. Sotiropoulos, "An integrated approach to correction for off-resonance effects and subject movement in diffusion MR imaging," *NeuroImage*, vol. 125, pp. 1063–1078, Jan. 2016. DOI: 10.1016/j.neuroimage.2015.10.019.

[59] S. M. Smith *et al.*, "Advances in functional and structural mr image analysis and implementation as fsl," *NeuroImage*, vol. 23, S208–S219, 2004. DOI: 10.1016/j.neuroimage.2004.07.051.

[60] K. G. Schilling *et al.*, "Synthesized b0 for diffusion distortion correction (synb0-disco)," *Magnetic Resonance Imaging*, vol. 64, pp. 62–70, 2019. DOI: 10.1016/j.mri.2019.05.008.

[61] MRtrix3 Documentation. "Multi-shell multi-tissue constrained spherical deconvolution," Accessed: May 27, 2026. [Online]. Available: https://mrtrix.readthedocs.io/en/latest/constrained_spherical_deconvolution/multi_shell_multi_tissue_csd.html.

[62] MRtrix3 Documentation. "Tckgen: Generate streamlines by tractography," Accessed: May 27, 2026. [Online]. Available: https://mrtrix.readthedocs.io/en/dev/reference/commands/tckgen.html.

[63] V. Lahy, *Structural connectivity analysis pipeline for alzheimer's disease*, https://github.com/valentinelahy/code, Accessed: 2026-05-25, 2026.

[64] E. Garyfallidis *et al.*, "Dipy, a library for the analysis of diffusion mri data," *Frontiers in Neuroinformatics*, vol. 8, p. 8, 2014. DOI: 10.3389/fninf.2014.00008.

[65] PiLAB Medical Imaging. "Registration: Mri registration pipeline," Accessed: May 27, 2026. [Online]. Available: https://github.com/PiLAB-Medical-Imaging/registration.

[66] B. Heifets. "Unravel: Unified nodal representation of axonal volume and connectivity estimation library," Accessed: May 27, 2026. [Online]. Available: https://github.com/b-heifets/UNRAVEL.

[67] M. S. Salman, T. D. Wager, E. Damaraju, and V. D. Calhoun, "An approach to automatically label & order brain activity/component maps," *bioRxiv*, 2020. DOI: 10.1101/2020.08.31.275578.

[68] NetworkX Developers. "Networkx documentation: Tutorial," Accessed: May 27, 2026. [Online]. Available: https://networkx.org/documentation/stable/tutorial.html.

[69] J. Guillon *et al.*, "Disrupted core-periphery structure of multimodal brain networks in alzheimer's disease," *Network Neuroscience*, vol. 3, no. 2, pp. 635–652, 2019. DOI: 10.1162/netn_a_00087.

[70] S. Ereira, S. Waters, A. Razi, and C. R. Marshall, "Early detection of dementia with default-mode network effective connectivity," *Nature Mental Health*, vol. 2, pp. 787–800, 2024. DOI: 10.1038/s44220-024-00259-5.

[71] Y. Song *et al.*, "Functional mri-specific alterations in salience network in mild cognitive impairment: An ale meta-analysis," *Frontiers in Aging Neuroscience*, vol. 13, p. 695 210, 2021. DOI: 10.3389/fnagi.2021.695210.

[72] I. Aganj *et al.*, "Compensatory brain connection discovery in alzheimer's disease," in *Proceedings of the IEEE International Symposium on Biomedical Imaging (ISBI)*, 2020, pp. 283–287. DOI: 10.1109/ISBI45749.2020.9098440.

[73] V. Karpychev *et al.*, "Greater volumes of a callosal sub-region terminating in posterior language-related areas predict a stronger degree of language lateralization: A tractography study," *PLOS ONE*, vol. 17, no. 12, e0276721, 2022. DOI: 10.1371/journal.pone.0276721.

[74] Kenhub. "Gyrus cingulaire," Accessed: May 29, 2026. [Online]. Available: https://www.kenhub.com/fr/library/anatomie/gyrus-cingulaire.

[75] A. Yamaguchi and T. Jitsuishi, "Structural connectivity of the precuneus and its relation to resting-state networks," *Neuroscience Research*, vol. 209, pp. 9–17, 2024. DOI: 10.1016/j.neures.2023.12.004.

[76] A. E. Cavanna and M. R. Trimble, "The precuneus: A review of its functional anatomy and behavioural correlates," *Brain*, vol. 129, no. 3, pp. 564–583, 2006. DOI: 10.1093/brain/awl004.

[77] Nature Index. "Subcortical mechanisms in language processing." Accessed May 18, 2026, Accessed: May 18, 2026. [Online]. Available: https://www.nature.com/nature-index/topics/l4/subcortical-mechanisms-in-language-processing.

[78] M. Catani, D. K. Jones, and D. H. Ffytche, "Perisylvian language networks of the human brain," *Annals of Neurology*, vol. 57, no. 1, pp. 8–16, 2005. DOI: 10.1002/ana.20319.

[79] F. Zong, Z. You, L. Zhou, and X. Deng, "Language function of the superior longitudinal fasciculus in patients with arteriovenous malformation as evidenced by automatic fiber quantification," *Frontiers in Radiology*, vol. 3, p. 1 121 879, 2023. DOI: 10.3389/fradi.2023.1121879.

[80] Wikipédia. "Faisceau arqué," Accessed: May 29, 2026. [Online]. Available: https://fr.wikipedia.org/wiki/Faisceau_arqu%C3%A9.

[81] J. Sobotta. "Sobo 1909 670 – superior longitudinal fasciculus." Image accessed via Wikimedia Commons/Wikipedia, Accessed: May 29, 2026. [Online]. Available: https://fr.wikipedia.org/wiki/Fichier:Sobo_1909_670_-_Superior_longitudinal_fasciculus.png.

[82] B. W. Fling, B. L. Benson, and R. D. Seidler, "Transcallosal sensorimotor fiber tract structure–function relationships," *Human Brain Mapping*, vol. 34, no. 2, pp. 384–395, 2013. DOI: 10.1002/hbm.21437.

[83] J. Andrade-Guerrero *et al.*, "Alzheimer's disease: Understanding motor impairments," *Brain Sciences*, vol. 14, no. 11, p. 1054, 2024. DOI: 10.3390/brainsci14111054.

[84] C. Metzler-Baddeley, D. K. Jones, J. Steventon, L. Westacott, J. P. Aggleton, and M. J. O'Sullivan, "Cingulum microstructure predicts cognitive control in older age and mild cognitive impairment," *The Journal of Neuroscience*, vol. 32, no. 49, pp. 17 612–17 619, 2012. DOI: 10.1523/JNEUROSCI.3299-12.2012.

[85] M. Bozzali *et al.*, "Damage to the cingulum contributes to alzheimer's disease pathophysiology by deafferentation mechanism," *Human Brain Mapping*, vol. 33, no. 6, pp. 1295–1308, 2012. DOI: 10.1002/hbm.21287.

[86] Wikipedia contributors. "Cingulum (cerebrum)," Accessed: May 29, 2026. [Online]. Available: https://la.wikipedia.org/wiki/Cingulum_(cerebrum).

[87] W. de Haan *et al.*, "Functional neural network analysis in frontotemporal dementia and alzheimer's disease using eeg and graph theory," *BMC Neuroscience*, vol. 10, p. 101, 2009. DOI: 10.1186/1471-2202-10-101.

[88] E. Bullmore and O. Sporns, "Complex brain networks: Graph theoretical analysis of structural and functional systems," *Nature Reviews Neuroscience*, vol. 10, no. 3, pp. 186–198, 2009.

[89] B. M. Tijms *et al.*, "Alzheimer's disease: Connecting findings from graph theoretical studies of brain networks," *Neurobiology of Aging*, vol. 34, no. 8, pp. 2023–2036, 2013. DOI: 10.1016/j.neurobiolaging.2013.02.020.

Appendix A

Inventory: Missing Data

A total of 186 participants were initially available in the dataset. However, some participants had missing demographic or imaging data and therefore had to be excluded from specific analyses. Table A.1 summarizes the missing data and final exclusions applied throughout the study.

Table A.1: Summary of missing demographic information, imaging data availability, and participant exclusions across the study.

Category	Number of participants
Clinical and demographic information	
Missing MRI acquisition date	2
Missing sex information	0
Missing education years	9
Missing diagnostic classification	3
Missing demographic covariates	11
MRI visit not found in Excel database	2
MRI and tractography data availability	
Missing tractogram	9
Missing connectivity matrix	11
Missing FA image	3
Missing brain mask	2
Missing label volume	2
Final number included in unadjusted analyses	173
Final number included in adjusted analyses	163

Participants Excluded from Unadjusted Analyses

Participant	Reason for exclusion
TAU_102_ses-1	Missing tractogram
TAU_121_ses-0	Missing tractogram
TAU_159_ses-0	Missing tractogram
TAU_238_ses-0	Missing tractogram
TAU_239_ses-0	Missing tractogram + missing date of birth
TAU_38_ses-2	Missing tractogram
TAU_41_ses-1	Missing tractogram
TAU_50_ses-0	Missing tractogram
TAU_57_ses-0	Missing tractogram
TAU_95_ses-0	Missing connectivity matrix (SIFT2)
TAU_25_ses-2	Missing connectivity matrix (SIFT2)
TAU_240_ses-0	Missing information in Excel
TAU_241_ses-0	Missing information in Excel

Additional Participants Excluded from Adjusted Analyses

Participant	Reason for exclusion
TAU_16_ses-2	Missing education years
TAU_213_ses-0	Missing education years
TAU_23_ses-0	Missing education years
TAU_38_ses-0	Missing education years
TAU_54_ses-0	Missing education years
TAU_56_ses-0	Missing education years
TAU_77_ses-0	Missing education years
TAU_230_ses-0	Missing education years
TAU_92_ses-05	Visit not found in Excel database
TAU_162_ses-05	Visit not found in Excel database

Appendix B

Cognitive Scores: p-values Comparisons

Table B.1: Post-hoc Tukey HSD comparisons between diagnostic groups for cognitive scores. Adjusted p-values are reported.

Score	**Comparison**	**Adjusted p-value**	**Significant**
MMSE	CN vs MCI	< 0.001	Yes
MMSE	CN vs Dementia	< 0.001	Yes
MMSE	MCI vs Dementia	< 0.001	Yes
Memory	CN vs MCI	< 0.001	Yes
Memory	CN vs Dementia	< 0.001	Yes
Memory	MCI vs Dementia	0.008	Yes
Language	CN vs MCI	< 0.001	Yes
Language	CN vs Dementia	< 0.001	Yes
Language	MCI vs Dementia	0.002	Yes
Executive	CN vs MCI	< 0.001	Yes
Executive	CN vs Dementia	< 0.001	Yes
Executive	MCI vs Dementia	< 0.001	Yes
Visuospatial	CN vs MCI	0.021	Yes
Visuospatial	CN vs Dementia	< 0.001	Yes
Visuospatial	MCI vs Dementia	< 0.001	Yes
Global cognitive	CN vs MCI	< 0.001	Yes
Global cognitive	CN vs Dementia	< 0.001	Yes
Global cognitive	MCI vs Dementia	< 0.001	Yes

Table B.2: Post-hoc Tukey HSD comparisons of global mean connectivity between diagnostic groups before and after covariate adjustment. Adjusted p-values are reported.

Analysis	**Comparison**	**Adjusted p-value**	**Significant**
Unadjusted	CN vs Dementia	0.0156	Yes
Unadjusted	CN vs MCI	0.2683	No
Unadjusted	MCI vs Dementia	0.2075	No
Adjusted	CN vs Dementia	0.0243	Yes
Adjusted	CN vs MCI	0.7438	No
Adjusted	MCI vs Dementia	0.0794	No

Table B.3: Post-hoc Tukey HSD comparisons of DMN connectivity between diagnostic groups before and after covariate adjustment. Adjusted p-values are reported.

Analysis	**Comparison**	**Adjusted p-value**	**Significant**
Unadjusted	CN vs Dementia	0.7852	No
Unadjusted	CN vs MCI	0.2003	No
Unadjusted	MCI vs Dementia	0.8059	No
Adjusted	CN vs Dementia	0.9693	No
Adjusted	CN vs MCI	0.6150	No
Adjusted	MCI vs Dementia	0.8868	No

Table B.4: Post-hoc Tukey HSD comparisons of SN connectivity between diagnostic groups before and after covariate adjustment. Adjusted p-values are reported.

Analysis	**Comparison**	**Adjusted p-value**	**Significant**
Unadjusted	CN vs Dementia	0.0325	Yes
Unadjusted	CN vs MCI	0.0123	Yes
Unadjusted	MCI vs Dementia	0.9095	No
Adjusted	CN vs Dementia	0.0349	Yes
Adjusted	CN vs MCI	0.0234	Yes
Adjusted	MCI vs Dementia	0.8340	No

Table B.5: Post-hoc Tukey HSD comparisons of CEN connectivity between diagnostic groups before and after covariate adjustment. Adjusted p-values are reported.

Analysis	**Comparison**	**Adjusted p-value**	**Significant**
Unadjusted	CN vs Dementia	0.4352	No
Unadjusted	CN vs MCI	0.3589	No
Unadjusted	MCI vs Dementia	0.9718	No
Adjusted	CN vs Dementia	0.5260	No
Adjusted	CN vs MCI	0.5439	No
Adjusted	MCI vs Dementia	0.9456	No

Table B.6: Post-hoc Tukey HSD pairwise comparisons for mean strength connectivity metrics before and after adjustment for age, sex, and education. Significant adjusted p-values are shown in bold.

Analysis	Comparison	Mean difference	Adjusted p-value	Significant
Unadjusted	CN vs Dementia	-8.441	**0.0020**	Yes
Unadjusted	CN vs MCI	-6.947	**0.0005**	Yes
Unadjusted	Dementia vs MCI	1.494	0.805	No
Adjusted	CN vs Dementia	-7.197	**0.0088**	Yes
Adjusted	CN vs MCI	-5.467	**0.0064**	Yes
Adjusted	Dementia vs MCI	1.730	0.738	No

Table B.7: Post-hoc Tukey HSD pairwise comparisons for mean clustering coefficient before and after adjustment for age, sex, and education. Significant adjusted p-values are shown in bold.

Analysis	Comparison	Mean difference	Adjusted p-value	Significant
Unadjusted	CN vs Dementia	-0.0064	**0.0025**	Yes
Unadjusted	CN vs MCI	-0.0037	**0.0221**	Yes
Unadjusted	Dementia vs MCI	0.0027	0.315	No
Adjusted	CN vs Dementia	-0.0065	**0.0022**	Yes
Adjusted	CN vs MCI	-0.0026	0.150	No
Adjusted	Dementia vs MCI	0.0039	0.088	No

Table B.8: Post-hoc Tukey HSD pairwise comparisons for mean closeness centrality before and after adjustment for age, sex, and education. Significant adjusted p-values are shown in bold.

Analysis	Comparison	Mean difference	Adjusted p-value	Significant
Unadjusted	CN vs Dementia	-0.0841	**0.0044**	Yes
Unadjusted	CN vs MCI	-0.0753	**0.0004**	Yes
Unadjusted	Dementia vs MCI	0.0088	0.936	No
Adjusted	CN vs Dementia	-0.0721	**0.0146**	Yes
Adjusted	CN vs MCI	-0.0579	**0.0066**	Yes
Adjusted	Dementia vs MCI	0.0142	0.834	No

Table B.9: Post-hoc Tukey HSD pairwise comparisons for mean betweenness centrality before and after adjustment for age, sex, and education. Significant adjusted p-values are shown in bold.

Analysis	Comparison	Mean difference	Adjusted p-value	Significant
Unadjusted	CN vs Dementia	0.0006	**0.0051**	Yes
Unadjusted	CN vs MCI	0.0002	0.176	No
Unadjusted	Dementia vs MCI	-0.0003	0.141	No
Adjusted	CN vs Dementia	0.0005	**0.0439**	Yes
Adjusted	CN vs MCI	0.0002	0.355	No
Adjusted	Dementia vs MCI	-0.0003	0.318	No

Appendix C

Significant Tracts

This appendix provides the detailed list of selected significant structural connections identified in the edge-wise analyses for each cognitive score. For each score, the table reports the selected connections after FDR correction, together with the corresponding edge index, anatomical regions, corrected q-value, and regression coefficient. These tables complement the summary presented in the Results section and provide the full set of connections used for tract visualization and anatomical interpretation.

No.	Edge	Region 1	Region 2	q-value	Coeff.
1	(51,50)	Occipital_Mid_L	Occipital_Sup_R	0.0044	0.247
2	(47,46)	Lingual_L	Cuneus_R	0.0058	0.217
3	(59,50)	Parietal_Sup_L	Occipital_Sup_R	0.0069	0.298
4	(50,47)	Occipital_Sup_R	Lingual_L	0.0079	0.229
5	(61,58)	Parietal_Inf_L	Postcentral_R	0.0080	0.313
6	(50,49)	Occipital_Sup_R	Occipital_Sup_L	0.0089	0.190
7	(63,58)	SupraMarginal_L	Postcentral_R	0.0096	0.337
8	(67,50)	Precuneus_L	Occipital_Sup_R	0.0096	0.182
9	(57,4)	Postcentral_L	Frontal_Sup_R	0.0105	0.275
10	(5,4)	Frontal_Sup_Orb_L	Frontal_Sup_R	0.0117	0.280
11	(57,20)	Postcentral_L	Supp_Motor_Area_R	0.0128	0.299
12	(51,46)	Occipital_Mid_L	Cuneus_R	0.0145	0.158
13	(67,58)	Precuneus_L	Postcentral_R	0.0145	0.304
14	(84,52)	Temporal_Pole_Sup_R	Occipital_Mid_R	0.0145	0.185
15	(69,20)	Paracentral_Lobule_L	Supp_Motor_Area_R	0.0146	0.291

Table C.1: Selected significant structural connections for the Executive score.

No.	Edge	Region 1	Region 2	q-value	Coeff.
1	(59,50)	Parietal_Sup_L	Occipital_Sup_R	0.0017	0.313
2	(89,65)	Temporal_Inf_L	Angular_L	0.0025	0.237
3	(95,57)	Cerebelum_3_L	Postcentral_L	0.0025	0.232
4	(51,50)	Occipital_Mid_L	Occipital_Sup_R	0.0027	0.229
5	(67,58)	Precuneus_L	Postcentral_R	0.0047	0.331
6	(59,44)	Parietal_Sup_L	Calcarine_R	0.0047	0.289
7	(60,57)	Parietal_Sup_R	Postcentral_L	0.0047	0.374
8	(67,50)	Precuneus_L	Occipital_Sup_R	0.0047	0.186
9	(9,5)	Frontal_Mid_Orb_L	Frontal_Sup_Orb_L	0.0062	0.285
10	(68,59)	Precuneus_R	Parietal_Sup_L	0.0063	0.273
11	(89,61)	Temporal_Inf_L	Parietal_Inf_L	0.0067	0.241
12	(110,57)	Vermis_3	Postcentral_L	0.0067	0.236
13	(67,46)	Precuneus_L	Cuneus_R	0.0067	0.155
14	(57,4)	Postcentral_L	Frontal_Sup_R	0.0074	0.267
15	(68,54)	Precuneus_R	Occipital_Inf_R	0.0099	0.225

Table C.2: Selected significant structural connections for the Global cognition score.

No.	Edge	Region 1	Region 2	q-value	Coeff.
1	(89,65)	Temporal_Inf_L	Angular_L	0.0009	0.292
2	(83,49)	Temporal_Pole_Sup_L	Occipital_Sup_L	0.0022	0.191
3	(89,11)	Temporal_Inf_L	Frontal_Inf_Oper_L	0.0035	0.215
4	(89,61)	Temporal_Inf_L	Parietal_Inf_L	0.0040	0.294
5	(72,14)	Caudate_R	Frontal_Inf_Tri_R	0.0057	0.461
6	(77,15)	Thalamus_L	Frontal_Inf_Orb_L	0.0057	0.319
7	(47,15)	Lingual_L	Frontal_Inf_Orb_L	0.0060	0.197
8	(95,57)	Cerebelum_3_L	Postcentral_L	0.0061	0.250
9	(50,45)	Occipital_Sup_R	Cuneus_L	0.0097	0.216
10	(59,50)	Parietal_Sup_L	Occipital_Sup_R	0.0097	0.319
11	(90,64)	Temporal_Inf_R	SupraMarginal_R	0.0097	0.239
12	(89,1)	Temporal_Inf_L	Precentral_L	0.0105	0.202
13	(89,57)	Temporal_Inf_L	Postcentral_L	0.0125	0.191
14	(15,7)	Frontal_Inf_Orb_L	Frontal_Mid_L	0.0140	0.278
15	(39,1)	ParaHippocampal_L	Precentral_L	0.0155	0.268

Table C.3: Selected significant structural connections for the Language score.

No.	Edge	Region 1	Region 2	q-value	Coeff.
1	(95,57)	Cerebelum_3_L	Postcentral_L	0.0018	0.151
2	(83,57)	Temporal_Pole_Sup_L	Postcentral_L	0.0404	0.134
3	(105,57)	Cerebelum_9_L	Postcentral_L	0.0431	0.098
4	(39,31)	ParaHippocampal_L	Cingulum_Ant_L	0.0477	0.101
5	(89,65)	Temporal_Inf_L	Angular_L	0.0477	0.120

Table C.4: Selected significant structural connections for the Memory score.

No.	Edge	Region 1	Region 2	q-value	Coeff.
1	(51,50)	Occipital_Mid_L	Occipital_Sup_R	0.0007	0.104
2	(60,57)	Parietal_Sup_R	Postcentral_L	0.0079	0.146
3	(68,51)	Precuneus_R	Occipital_Mid_L	0.0090	0.046
4	(67,50)	Precuneus_L	Occipital_Sup_R	0.0119	0.071
5	(51,46)	Occipital_Mid_L	Cuneus_R	0.0138	0.062
6	(69,20)	Paracentral_Lobule_L	Supp_Motor_Area_R	0.0177	0.114
7	(50,49)	Occipital_Sup_R	Occipital_Sup_L	0.0185	0.068
8	(9,5)	Frontal_Mid_Orb_L	Frontal_Sup_Orb_L	0.0330	0.099
9	(59,50)	Parietal_Sup_L	Occipital_Sup_R	0.0330	0.100
10	(23,7)	Frontal_Sup_Medial_L	Frontal_Mid_L	0.0356	0.054
11	(60,4)	Parietal_Sup_R	Frontal_Sup_R	0.0356	0.058
12	(67,31)	Precuneus_L	Cingulum_Ant_L	0.0356	0.038
13	(67,58)	Precuneus_L	Postcentral_R	0.0356	0.111
14	(84,52)	Temporal_Pole_Sup_R	Occipital_Mid_R	0.0389	0.063
15	(61,58)	Parietal_Inf_L	Postcentral_R	0.0391	0.102

Table C.5: Selected significant structural connections for the MMSE score.

No.	Edge	Region 1	Region 2	q-value	Coeff.
1	(50,49)	Occipital_Sup_R	Occipital_Sup_L	0.0015	0.156
2	(59,44)	Parietal_Sup_L	Calcarine_R	0.0021	0.240
3	(51,46)	Occipital_Mid_L	Cuneus_R	0.0031	0.131
4	(68,59)	Precuneus_R	Parietal_Sup_L	0.0032	0.223
5	(51,50)	Occipital_Mid_L	Occipital_Sup_R	0.0056	0.168
6	(51,44)	Occipital_Mid_L	Calcarine_R	0.0152	0.086
7	(59,50)	Parietal_Sup_L	Occipital_Sup_R	0.0152	0.202
8	(20,1)	Supp_Motor_Area_R	Precentral_L	0.0172	0.279
9	(49,46)	Occipital_Sup_L	Cuneus_R	0.0216	0.110
10	(67,58)	Precuneus_L	Postcentral_R	0.0216	0.217
11	(57,20)	Postcentral_L	Supp_Motor_Area_R	0.0273	0.204
12	(63,58)	SupraMarginal_L	Postcentral_R	0.0273	0.220
13	(68,51)	Precuneus_R	Occipital_Mid_L	0.0273	0.077
14	(58,57)	Postcentral_R	Postcentral_L	0.0275	0.281
15	(4,1)	Frontal_Sup_R	Precentral_L	0.0334	0.262

Table C.6: Selected significant structural connections for the Visuospatial score.

UNIVERSITÉ CATHOLIQUE DE LOUVAIN
École polytechnique de Louvain
Rue Archimède, 1 bte L6.11.01, 1348 Louvain-la-Neuve, Belgique | **www.uclouvain.be/epl**